

國立臺灣大學理學院物理學研究所



碩士論文

Department of Physics

College of Science

National Taiwan University

Master Thesis

利用組織切片技術研究腦組織三維結構

Survey on Brain Tissue 3-D Reconstruction using different
Histology techniques

曾柏杭

Po-Hang Tseng

指導教授：董成淵 博士 黃佩欣 博士

Advisor: Chen-Yuan Dong Ph.D. Pei-Hsin Huang Ph.D.

中華民國 106 年 7 月

July, 2017

誌謝



能完成這篇論文除了自己的付出以外非常幸運的也得到很多人的幫助與鼓勵。一直到研究所第二學年快結束的前幾個月論文的完成仍然遙遙無期。謝謝董成淵老師與黃佩欣老師在關鍵時期引導我一步一步寫完這篇論文。謝謝陳永芳、張顏暉教授參與口試並且提出重要問題讓我看到自己的研究盲點。謝謝林宏銘學長與我共苦做實驗以及教我如何做實驗結果分析。謝謝黃旭成與李聖林學長在我失去研究方向的時候鼓勵我還有給我很有用的建議。

這兩年非常感謝董老師願意讓我參與腦科學的研究並且不時給予我做新研究的機會。在董老師的實驗室做研究讓我學到做事情的方法以及應有的態度。實驗室遇到問題時大家一起與老師解決讓我意識到團隊合作的重要性以及一個人力量的極限。雖然平常做實驗寧願自己在沒有人的時候默默完成實驗室的任務，卻發現經常會碰到問題，而與實驗室夥伴一起做事時反而可以減輕個人負擔並且在不同觀點分析同一件事的情況下非常有效率的找到問題最好的解決方式。我認真體悟到自己做事時會想要力求完美，但是這是客觀狀況所不允許，而與他人合作可以經由討論輕易看見問題所在與自己能力所及應該做的事情，並且不會因為個人的盲點使得研究無法進行。董老師在每次開會總是高度熱情並且與我們用討論的方式激發所有人思考如何解決問題。這兩年我從老師以及這個環境學到了積極樂觀看待實驗以及不輕易放棄的精神，畢竟沒有嘗試過失敗的實驗方法也不可能找到最佳解。

謝謝黃佩欣老師以及楊宗穎同學願意協助我做生物實驗讓基礎薄弱的我有機會在腦科學領域學習。謝謝南方科技李峰杰學長協助我們實驗室儀器的改良以及分享光學領域的知識。謝謝李聖林、林宏銘、黃旭成學長以及 Jen 教我做研究的基本常識與應有的態度，讓我有辦法順利進入況適應實驗環境。謝謝戰友林子翔很多地方都罩我或是在實驗很困難的時候跳出來幫忙。還有陪我做實驗的 Jen、明暉與 Minh，謝謝你們幫我分擔實驗的壓力，與我討論讓我檢驗自己對實驗過程的考慮是否有漏洞。謝謝兩位強大的助理陳彥妤、溫書涵包辦實驗室大小事情，你們處理行政以及實驗事物的周全與效率值得我向你們看齊。謝謝黃旭成與林宏銘學長盡心盡力照顧實驗室大小器材，讓大家可以放心做實驗。謝謝畢業學長姐

Connie、雅琳、羅伊、學聖，你們走過的路傳承給我們讓我們研究更有方向實驗更有效率。謝謝這兩年來家人朋友的鼓勵與陪伴，讓我能堅持下去走完這段人生旅程。



曾柏杭 於 2017 年 8 月 24 號

中文摘要



前腦發育畸形症屬稀罕人腦疾病，胎兒發育期間會發展出不正常的腦室，可依據不同的腦室變形程度加以分類。得此病最嚴重的情況胎兒只會有一個腦室，無法順利發育雙眼與鼻子。通常胎兒發育期間最先會由醫學超音波檢查診斷出該疾病，在最嚴重的情況下出生後無法存活。根據病理學，研究異常人體器官取下之組織樣本時須將組織切片並且由光學顯微鏡在小於釐米尺度的範圍觀察切片的細節。在本研究中，我們利用連續石蠟切片染色後由高解析度白光顯微鏡分析組織切片，並試著比較正常與前腦發育畸形之胎兒腦組織在二維及三維結構上的差異。另外我們也希望透過新型振動式切片技術與雙光子顯微技術的結合發展出更好的腦組織三維完整取像方法。使用任何方式進行組織切片時都會有組織損失的問題，進而增加三維影像接合之變數，本文亦將探討此問題對三維結構重建之影響。

關鍵字： 前腦發育畸形症、振動式切片技術、組織病理學、人腦、雙光子顯微技術

Abstract



Holoprosencephaly, a kind of brain disease, is usually identified by ultrasonography on fetuses during gestation and confirmed by Magnetic Resonance Imaging (MRI). In the most severe cases the fetus carries craniofacial malformations Cyclopia and Proboscis above the eye with the nose absent.

In this research we use the standard histological method to study the microscopic anatomy of brain tissue from human postmortem fetal brain with the Holoprosencephaly disease. Consecutive paraffin slices stained with Hematoxylin and Eosin were imaged by light microscopy and the images were then reconstructed into 3D stacks for more information on the anatomy of the disease. We also study the possibility of using agarose for embedding brain tissue along with the oscillating blade cutting technique to obtain better 3D image from slices with two-photon microscopy.

Keywords: Holoprosencephaly, Oscillating Microtome, Human Fetal Brain, Histopathology, Two Photon Microscopy

CONTENTS

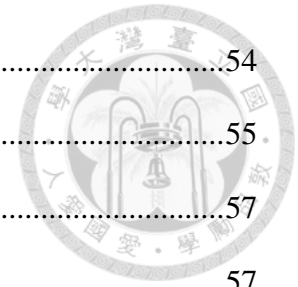


致謝	i
中文摘要	iii
Abstract.....	iv
CONTENTS	v
LIST OF FIGURES	viii
LIST OF TABLES	x
Chapter 1 Introduction.....	1
1.1 Motivation.....	1
1.2 Experimental Approach	3
Chapter 2 The Brain	5
2.1 Anatomical Reference	5
2.2 Basic Structure.....	7
2.2.1 Cerebrum.....	7
2.2.2 Cerebral Cortex and Layering	8
2.2.3 Hippocampus.....	10
2.2.4 Corpus Callosum.....	11
2.2.5 The Ventricular System	12
2.3 Congenital Brain Disease and Holoprosencephaly.....	13
2.3.1 Anencephaly.....	14
2.3.2 Lissencephaly	14
2.3.3 Holoprosencephaly.....	15
Chapter 3 The Standard Histology Approach.....	18

3.1	Brain Histology and Histopathology	18
3.1.1	Fixation	20
3.1.2	Paraffin Embedding.....	21
3.1.3	Tissue Sectioning with Microtome.....	22
3.1.4	Hematoxylin and Eosin Staining.....	23
3.1.5	Light Microscopy	24
3.2	Methods	26
3.2.1	Sample Preparation	26
3.2.2	Experimental Setup for Light Microscopy.....	27
3.2.3	Experiment Procedure	28
3.3	Results and Discussion	29
3.3.1	Histological Findings from 2-D Images.....	29
3.3.2	3-D Analysis of 20 Consecutive Tissue Slices	32
3.3.3	Discussion	41
Chapter 4	The Fresh tissue Approach.....	43
4.1	Overview of Alternative Histology.....	43
4.1.1	Agarose	44
4.1.2	The Pig Brain	45
4.2	The Flexure-Based Oscillating Blade System	46
4.2.1	Design of the modified vibrating Microtome.....	46
4.2.2	Cutting Parameters	48
4.2.3	Blade Material	48
4.2.4	Surface Roughness	51
4.3	Two-Photon Microscopy	52
4.3.1	Fluorescence.....	52



4.3.2	Two-Photon Fluorescence	54
4.3.3	Fluorescent Dyes and DAPI.....	55
4.4	Methods	57
4.4.1	Sample preparation.....	57
4.4.2	Setup of the Oscillating Blade System and Two-Photon LSM	58
4.4.3	Experiment Procedure	60
4.5	Results and Discussion	61
4.5.1	Steel Blade.....	62
4.5.2	Sapphire Blade	63
4.5.3	Tungsten Carbide Blade	64
4.5.4	Discussion	64
Chapter 5	Conclusion	66
5.1	Comparison of the Histology Techniques.....	66
5.2	Present Limitations and Future Work	67
	REFERENCE	69

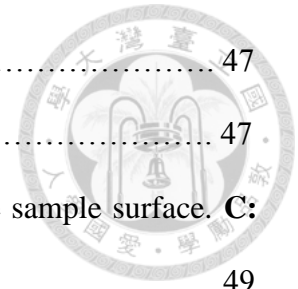


LIST OF FIGURES



Fig. 1.1 Experimental approach to 3-D Histology.....	4
Fig. 2.1 Sectional planes of the brain	6
Fig. 2.2 Basic structures of the brain	8
Fig. 2.3 Cerebral cortex of human fetus 6 months	10
Fig. 2.4 Hippocampus of monkey enhanced with Nissl stain	11
Fig. 2.5 Basic morphology of the ventricular system	13
Fig. 2.6 Alobar holoprosencephaly, MRI at 0.5T	14
Fig. 2.7 Embryology of Holoprosencephaly	16
Fig. 2.8 Classification of Holoprosencephaly	16
Fig. 3.1 Steps for Practicing Histopathology	19
Fig. 3.2 Crosslinking mechanism of formaldehyde with protein	21
Fig. 3.3 LEICA Microtome RM2125 RTS	22
Fig. 3.4 Chemical formulae	24
Fig. 3.5 Overview of the Holoprosencephaly(A10654) brain after fixation	27
Fig. 3.6 Experimental setup for light microscope imaging	28
Fig. 3.7 Comparison of neocortex structure between control and disordered brain stained with H&E	31
Fig. 3.8 Dentate gyrus, A10654	32
Fig. 3.9 Results of control A10642	35
Fig. 3.10 Results for the holoprosencephaly A10654	38
Fig. 3.11 Results for the hippocampus of holoprosencephaly A10654	41
Fig. 4.1 Chemical structure of agarose	44
Fig. 4.2 Pig brain in 10% formalin	46

Fig. 4.3 Process of optimizing blade motion	47
Fig. 4.4 Top view of the oscillating blade system	47
Fig. 4.5 A: Optimum knife angle. B: Angle too low; knife hits the sample surface. C: Angle too steep; sample slice above the knife is pushed	49
Fig. 4.6 Mechanism of fluorescence	53
Fig. 4.7 Jablonski Diagrams	54
Fig. 4.8 TPLSM achieves better focus and penetration depth compared to CLSM	55
Fig. 4.9 DAPI	56
Fig. 4.10 Meninges on pig brain	58
Fig. 4.11 Embedding with the constraint	58
Fig. 4.12 The oscillating blade system	59
Fig. 4.13 Two-photon LSM system (figure provided by Ya-Lin Huang)	60
Fig. 4.14 Experiment blades	61
Fig. 4.15 Steel without constraint	62
Fig. 4.16 Steel with constraint	62
Fig. 4.17 Sapphire without constraint	63
Fig. 4.18 Sapphire with constraint	63
Fig. 4.19 Tungsten carbide without constraint	64
Fig. 4.20 Tungsten carbide with constraint	64



LIST OF TABLES



Table 4.1 Mohs hardness scale 51

Chapter 1 Introduction

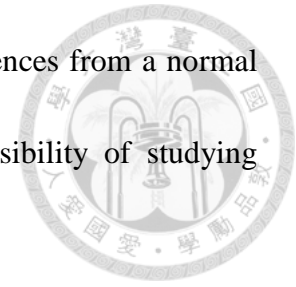


The brain is one of the most important organ in our body. It is the master of all behavior and also interprets and controls all the sensory experience from the world in our everyday lives. Due to the importance it bares the brain is composed of morphologically complex structures with multiple functions. Of all the organs in the human body, the structure of the brain puzzled observers in the past the most [1]. If the brain is damaged in anyway or improperly grown during prenatal development it will cause severe consequences including death. According to estimates from the World Health Organization (WHO), more than ten percent of world mortality is caused by neurological disorders [2]. This stresses the importance of brain research and brain pathology to improve the lives of people all around the world.

1.1 Motivation

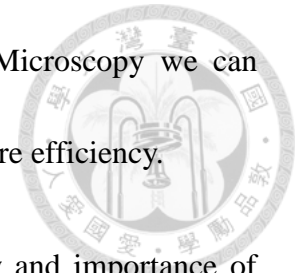
It is estimated that every year about 6% of newborn babies in the world are born with congenital defects and over 50% of these defects the cause is unknown [3]. Holoprosencephaly, a neurological congenital disorder, occurs at the rate of about 1.31:10,000 [4]. The traits of the disease are identified by ultrasonography during pregnancy and the final diagnosis is usually confirmed by Magnetic Resonance Imaging (MRI). To study the disease, histopathological techniques such as paraffin embedded

sectioning with molecular labeling were used to identify the differences from a normal fetal brain [5]. The purpose of this thesis is to discuss the possibility of studying histopathological information in a three dimensional point of view.



Macroscopic diagnosis of the brain can be done by the Magnetic Resonance Imaging technique (MRI) can take serial images of different depth of the human brain and 3-D reconstruction is possible but high resolution cannot be achieved. To study abnormal brain tissues on the microscopic scale we use the paraffin embedding technique followed by Hematoxylin and Eosin stains (H&E) and image micrographs for diagnosis. With H&E staining and observation by a light microscope each slice only contains two dimensional information. However, if consecutive paraffin sections are done, we can still reconstruct three dimensional images from the 2-D slice images as a stack with the slice thickness being the resolution in the z-axis direction. This technique, however, is still limited by the slice thickness in that paraffin slices prepared are usually not thicker than 20 μm [6]. Also, the thicker we slice the lower the resolution we have in the z-direction. Therefore it is technically difficult to get 3-D information from thick tissue blocks with about 1cm thickness as we may need to cut hundreds of serial sections with the Microtome without stopping in the middle. An alternative choice for obtaining 3-D image is to embed brain tissue into agarose without dehydrating and then use a flexure-based oscillating blade system designed by Professor Shih Chi Chen from The Chinese University of Hong Kong to take thick tissue sections [7]. With this

technique combined with fluorescent labeling and Two Photon Microscopy we can section with higher thickness above 100 μm and image 3-D with more efficiency.



The goal of this study therefore is to evaluate the possibility and importance of bringing 3-D microscale analysis into studying congenital brain disorders such as Holoprosencephaly. We hope to discover new traits or structures that cannot be analyzed by a single 2-D tissue slice and provide another tool for studying brain histopathology.

1.2 Experimental Approach

There will be two approaches of this study to get 3-D information from the brain (**Fig. 1.1**). The first part of the thesis (Chapter3) will be about the paraffin sectioning method that is commonly referred to as standard histology. Twenty consecutive paraffin embedded sections were sliced by Microtome for both the holoprosencephaly brain and control brain. The slices were then placed on glass slides and stained with H&E to be imaged by a CCD camera connected to an optical microscope objective lens. Finally, the images were matched to one another rotationally and translationally before 3D image is reconstructed. In the second part (Chapter4) we investigated the possibility of cutting brain tissue with more thickness and without dehydrating the sample. We embedded formalin fixed brain samples with agarose and used a flexure-based oscillating blade system to cut thicker sections (about 300 μm). We then used Two Photon Microscopy for imaging the surface of the thick brain slices and calculating the

surface roughness.

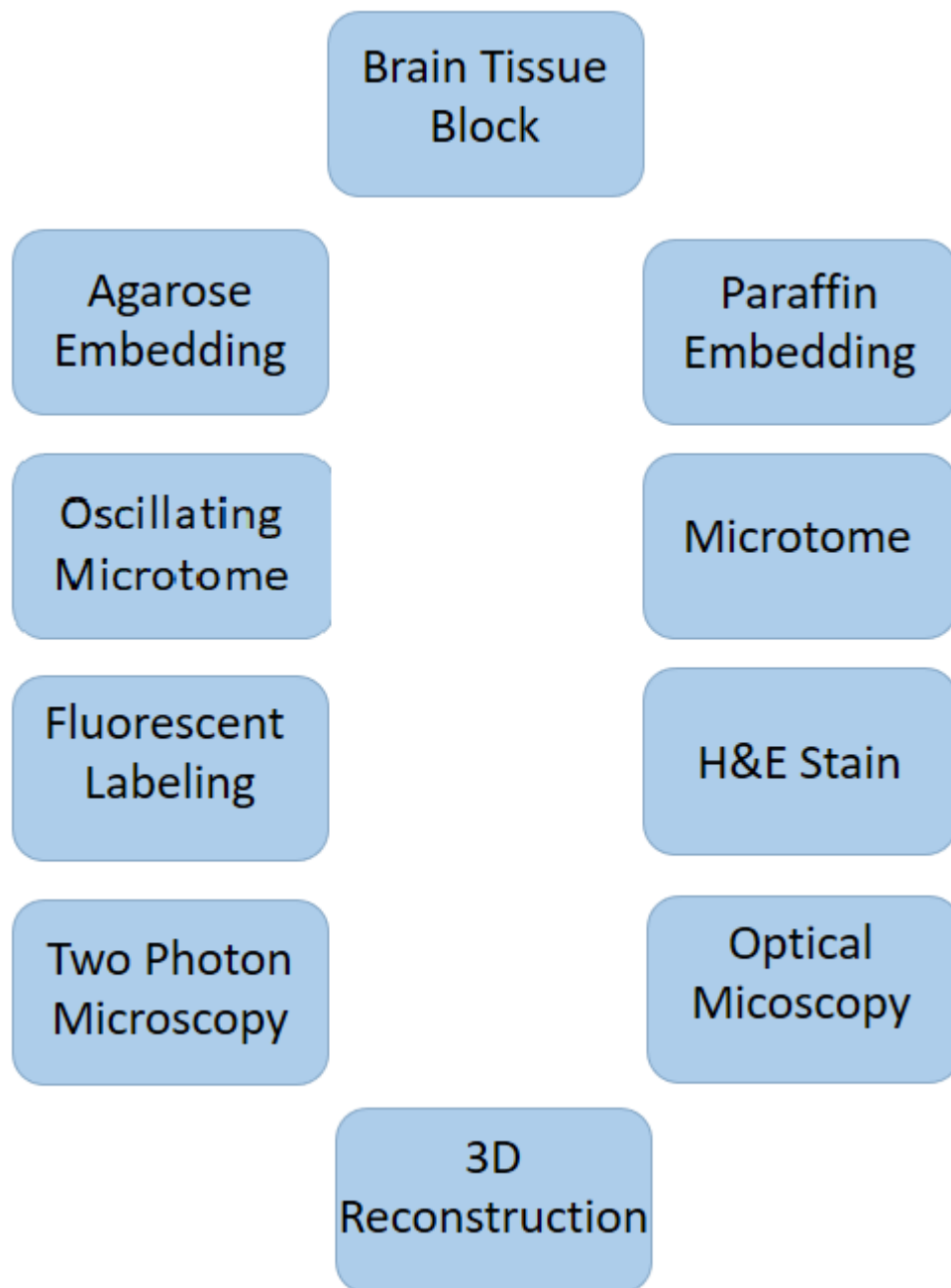


Fig. 1.1 Experimental approach to 3-D Histology

Chapter 2 The Brain



2.1 Anatomical Reference

The human body possesses bilateral symmetry and so does the human brain. This means that the brain has one plane of symmetry and it can divide the brain roughly into the left and right part macroscopically. There are three ways of looking at a brain on a 2-D plane [8]:

Coronal Plane – The plane that is parallel to the chest and face and is perpendicular to the plane of symmetry.

Sagittal Plane – The plane that is parallel to the plane of symmetry. There is a name for the plane of symmetry called the Midsagittal plane since it divides the brain into two equal parts macroscopically by sectioning at the middle.

Horizontal Plane – The plane that is parallel to the ground when we are standing and is perpendicular to the other two sectional planes.

The three sectional planes demonstrated on a mouse brain is shown in **Fig. 2.1**



Coronal Plane



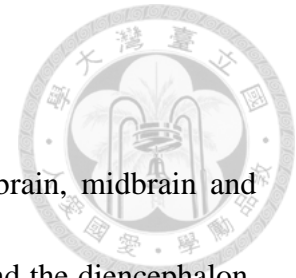
Sagittal Plane



Horizontal Plane

Fig. 2.1 Sectional planes of the brain [8]

2.2 Basic Structure

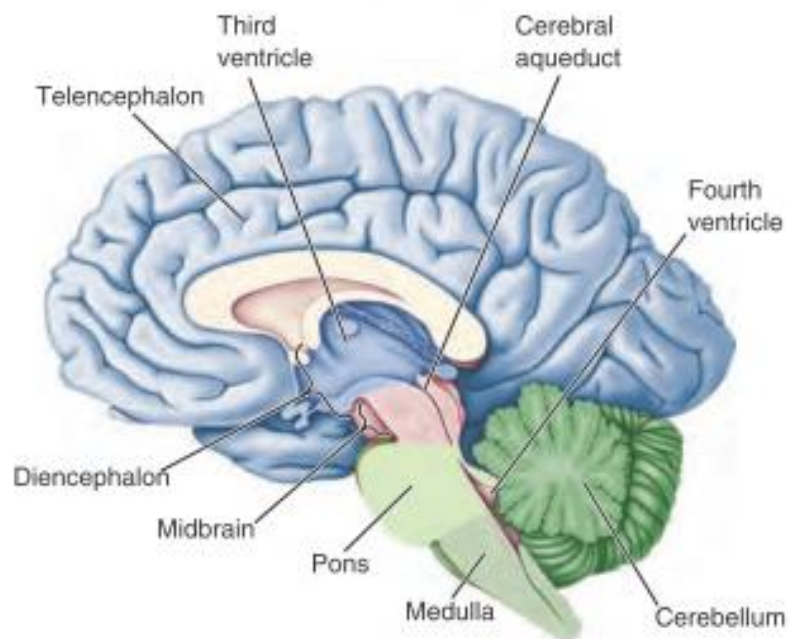


The brain at fetal development can be divided into the forebrain, midbrain and hindbrain. The forebrain is further divided into the telencephalon and the diencephalon.

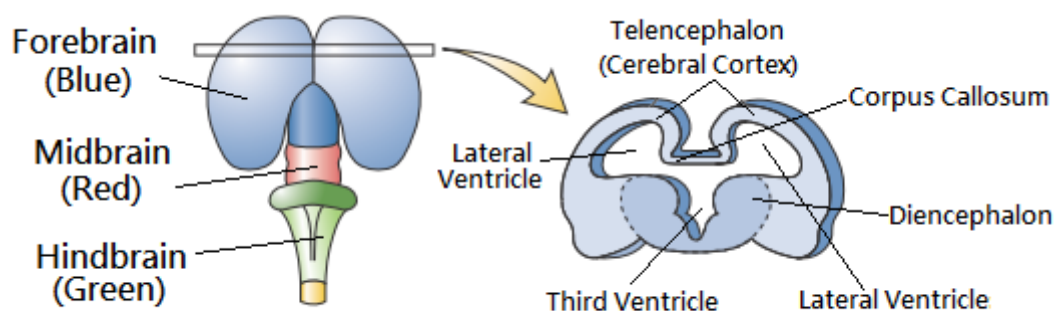
The telencephalon grows into the cerebrum and the diencephalon grows mainly into the thalamus and hypothalamus. The brain also has a ventricular system divided into four chambers containing cerebrospinal fluid (CSF) and linked to the spinal cord. The basic structures of the brain are shown in **Fig. 2.2**.

2.2.1 Cerebrum

The cerebrum is the largest and also the most important part of the brain. It is responsible for our long term memory [9] and also integrates the information we receive from the outside world by our sense organs. The cerebrum is composed of white matter and grey matter. The white matter is the inner part of the cerebrum and is composed mainly of myelinated axons. The grey matter, also known as the cerebral cortex, is the outer part of the cerebrum and is responsible for the main functions of the cerebrum owing to the fact that the majority of neuronal cell bodies lies within this region.



(a)



(b)

Fig. 2.2 Basic structures of the brain. (a) Brain sagittal overview. (b) Coronal view of the forebrain. [8]

2.2.2 Cerebral Cortex and Layering

The mature human cerebral cortex, also known as the gray matter, is about one to a few millimeters thick and has six layers with different functions. The six layers from the

surface of the brain to the neighbor of the white matter are:

1st Layer: This is also called the Molecular Layer and cell density is considerably low compared to other layers.

2nd Layer: External Granular Layer

3rd Layer: The External Pyramidal Layer

4th Layer: The Inner Granular Layer.

5th Layer: The Inner Pyramidal Layer

6th Layer: Multiform Layer

German neurologist Dr. Korbinian Brodmann (1868 – 1918) in 1909 discussed the layering of the cortex thoroughly in his book about the cerebral cortex [10]. A graph of the six layers at the developmental stage of the human brain is shown in **Fig. 2.3**.



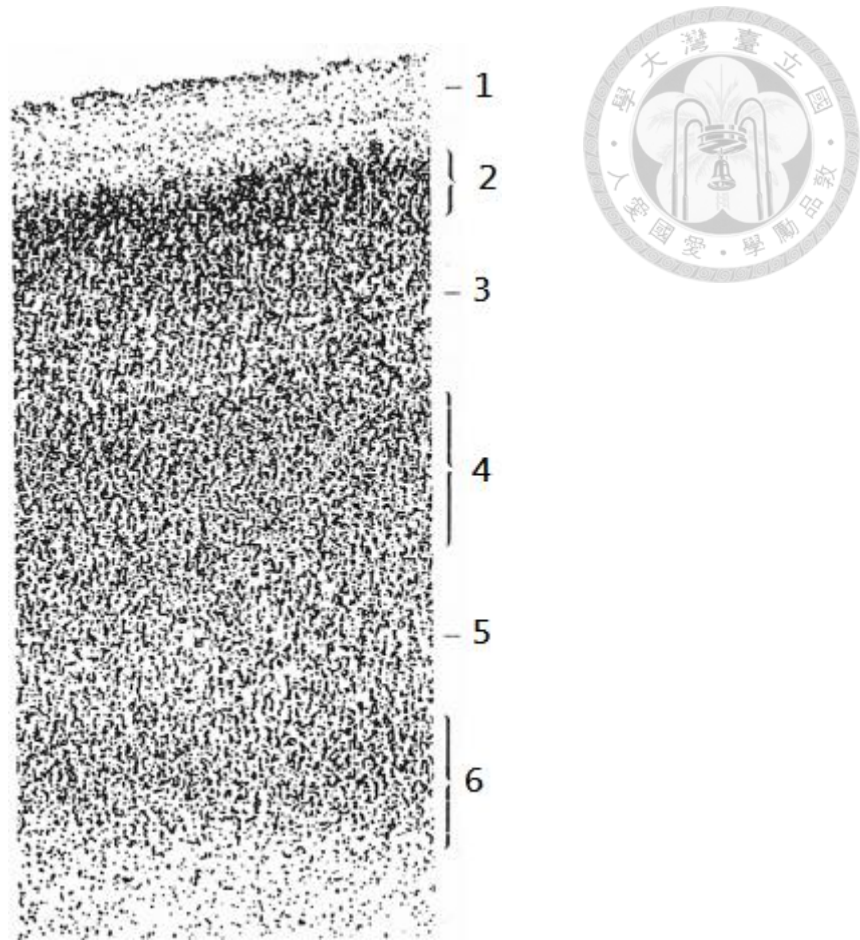


Fig. 2.3 Cerebral cortex of human fetus 6 months. Layers 2,4 and 6 have higher cell density. [10]

2.2.3 Hippocampus

The hippocampus is also a part of the brain cortex but is different from the cerebral cortex mentioned above. The cerebral cortex is also known as the neocortex and the hippocampus belongs to the allocortex family. The main difference from these two types of cortices is that the neocortex has six layers while the allocortex usually has three or four. The hippocampus is composed of the cornus ammonis (CA) regions and the dentate gyrus [11]. In **Fig. 2.4** we see that there is a dark layer for both the dentate gyrus

and the cornus ammonis, each representing a dense granule cell and pyramidal cell layer.

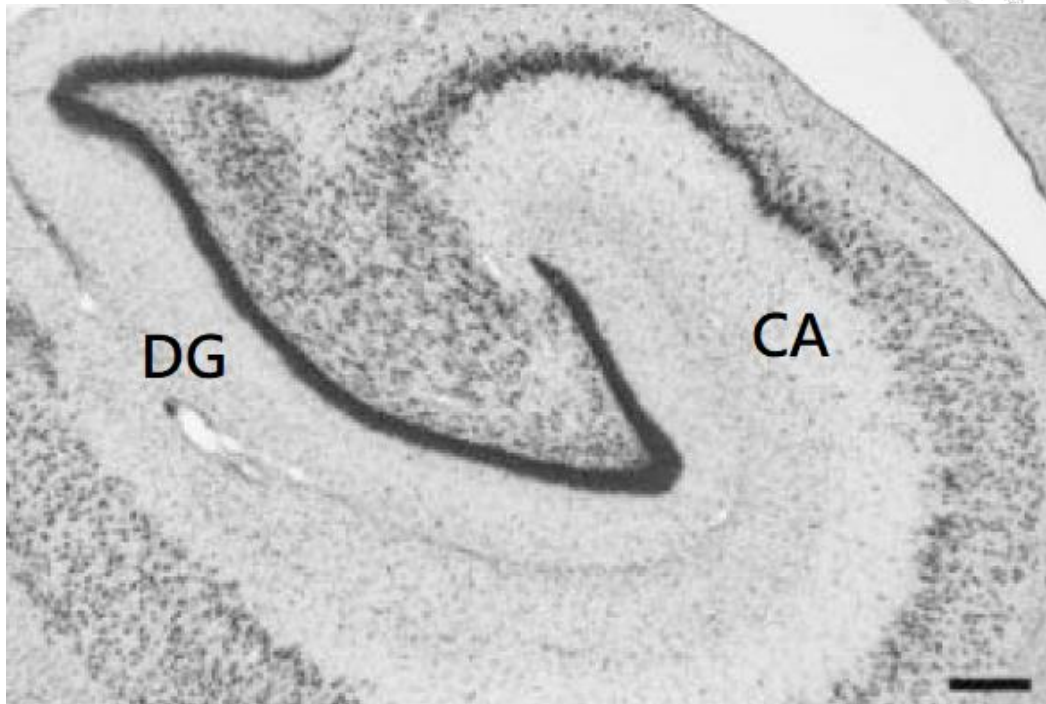
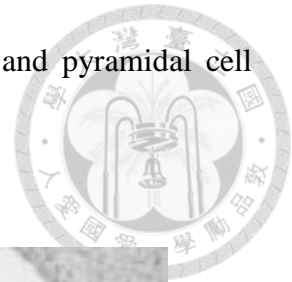
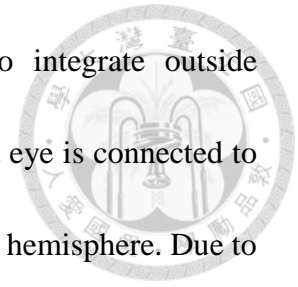


Fig. 2.4 Hippocampus of monkey enhanced with Nissl stain. DG: dentate gyrus; CA: cornus ammonis. Scale bar: 350 μm . [11]

2.2.4 Corpus Callosum

The corpus callosum is the white matter structure that connects the left and right cerebral hemispheres. Both hemispheres work as individuals with different functions and need to communicate with each other through the corpus callosum. If this structure is not working properly then the lack of information exchange from the two hemispheres may lead to severe consequences. The Split-Brain is a symptom of corpus

collasum disorder and results in the incapability of patients to integrate outside information as one whole brain. For a normal human brain the right eye is connected to the left cerebral hemisphere and the left eye is connected to the right hemisphere. Due to this fact, experiments were done by stimulating only one visual field (namely letting only one eye see) with simple words to test the response of the patients [12]. The results were that patients that received information only from the right brain hemisphere could not respond with specific functions of the left hemisphere such as speech.



2.2.5 The Ventricular System

This is the system of all the ventricles in the brain and is filled with cerebrospinal fluid (CSF). The CSF is produced by a structure called the choroid plexus containing modified ependymal cells. The human brain ventricular system consists of four ventricles each being responsible for protecting different regions of the brain (see **Fig. 2.5**).

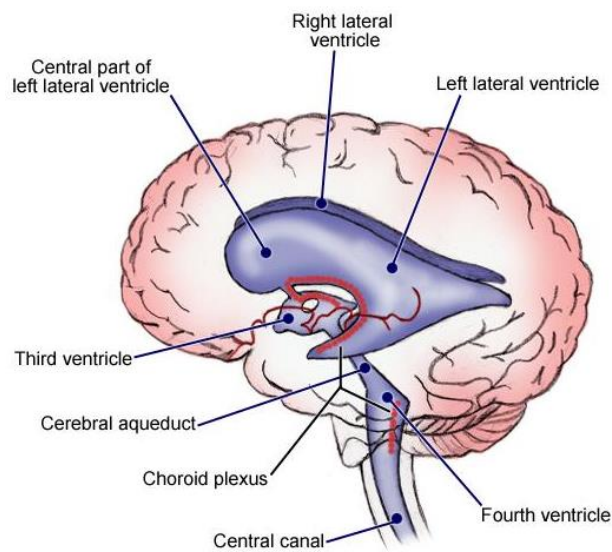


Fig. 2.5 Basic morphology of the ventricular system. [13]

2.3 Congenital Brain Disease and Holoprosencephaly

Congenital brain disorders are defined as the defects of the brain of a baby at birth compared to other newborn healthy babies. The disease is often discovered by ultrasonography and magnetic resonance imaging (MRI) (**Fig. 2.6**) at the fetal stage before birth and termination of the fetal life is done when necessary. In this section we introduce some common fetal brain diseases and discuss in more detail about the Holoprosencephaly disease.

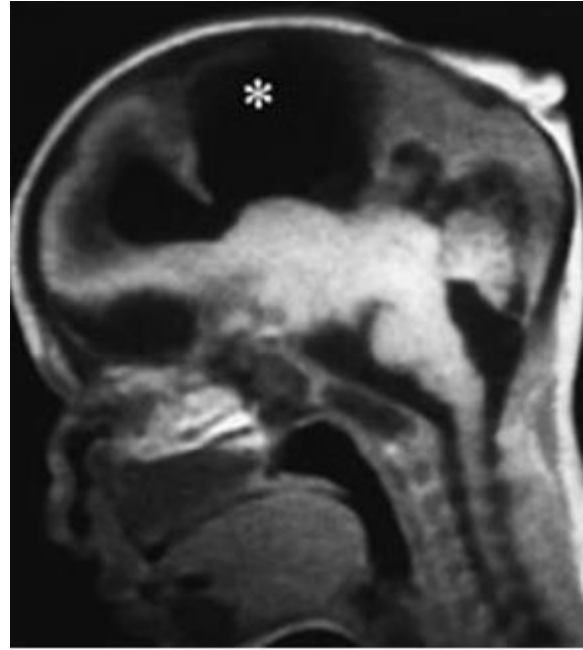


Fig. 2.6 Alobar holoprosencephaly, MRI at 0.5T. Asterisk: Large dorsal sac of holovertricle. [14]

2.3.1 Anencephaly

This is one of the most serious brain disorders and affects about 1,000 newborn infants in the United States every year [15]. Babies with this disease don't have a forebrain structure and the rest of the brain tissue is not protected by the skull and they do not survive after birth.

2.3.2 Lissencephaly

This structural brain disease that is diagnosed when the brain appears smooth at the surface different from a normal brain cortex characterized by a lot of sulci and gyri. Studies showed that this disorder resulted from impaired cell migration during the third

and fourth months of pregnancy [16].



2.3.3 Holoprosencephaly

Holoprosencephaly is a rare disease that induces structural defects on the forebrain of the fetus. The main feature of this disease would be that the cerebral hemisphere fails to separate into the left and right part and thus poor division of the lateral ventricles [17] (**Fig. 2.7**). Reviews of the severity of the disease in the past have classified it into three levels [18] (**Fig. 2.8**):

(1)**Lobar holoprosencephaly**: Clear signs of separate hemispheres and only incomplete growth of the forebrain.

(2)**Semilobar holoprosencephaly**: No separation of hemispheres at the forebrain but still a bit of incomplete division.

(3)**Alobar holoprosencephaly**: The brain fails to separate at all. This will cause serious facial distortion such as Cyclopia and usually the fetus dies before birth.

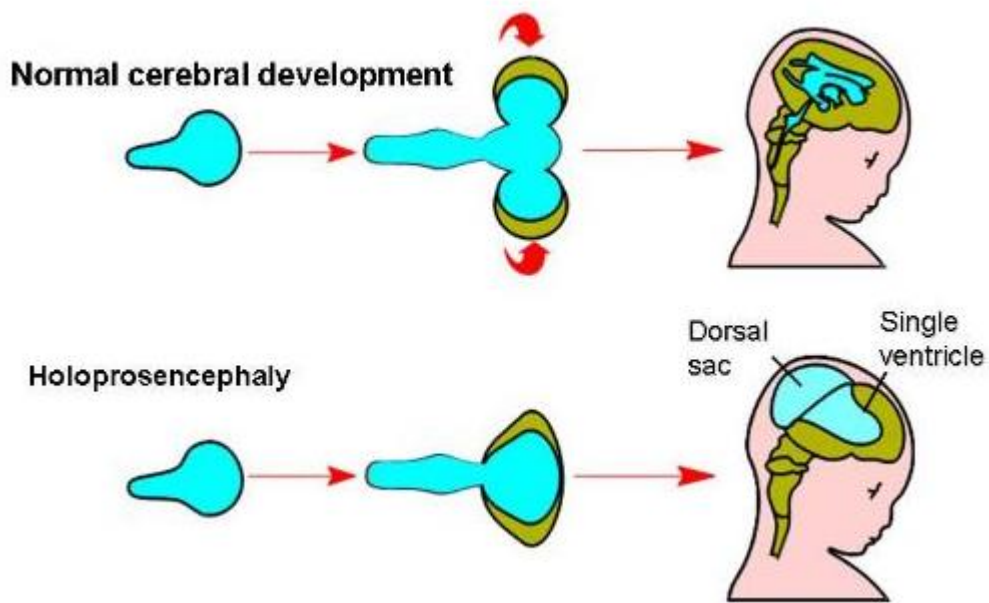


Fig. 2.7 Embryology of Holoprosencephaly (Image by G. Pilu) [17]

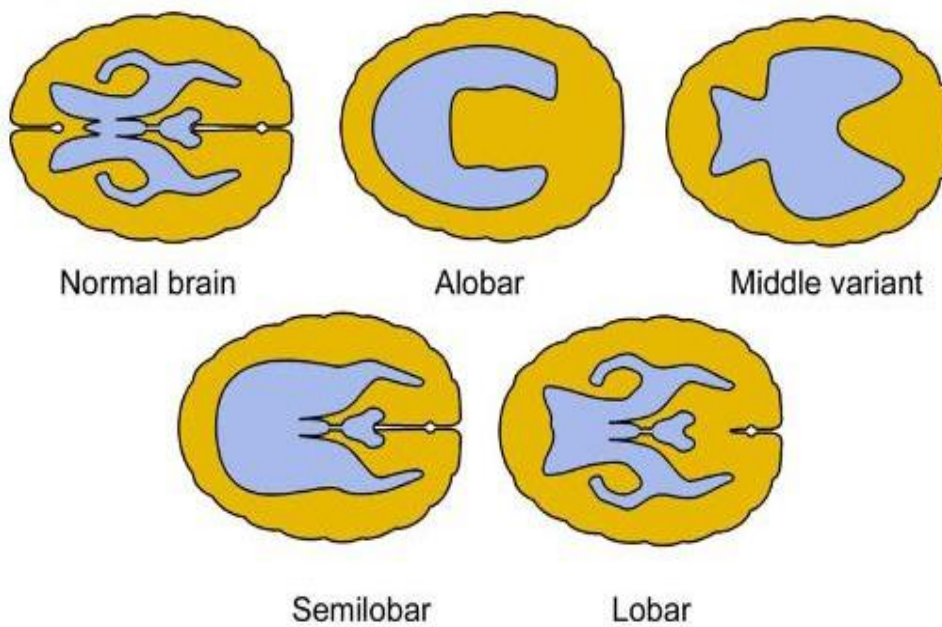
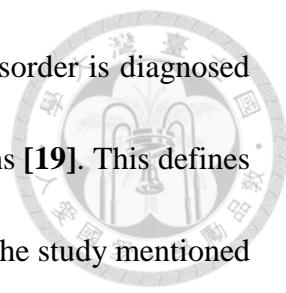


Fig. 2.8 Classification of Holoprosencephaly (Image by G. Pilu) [17]



Incidence: A study showed that the rate at which this brain disorder is diagnosed during pregnancy or on newborn infants is about 1-2 per 10,000 births [19]. This defines Holoprosencephaly as a rare disease but also a very lethal one since the study mentioned above also stated that in 80% of the cases pregnancy was terminated before giving birth to the child.

Histological Findings: The cortex of the fetal brain diagnosed with Holoprosencephaly were studied by histopathology and showed that the cell distribution was abnormal and lamination was unclear [5]. The study also showed typical structures where cells tend to circle around neurites to form a glomerular structure.

Chapter 3 The Standard Histology Approach



In This chapter we follow the standard procedure of histology and discuss the results of combining this with 3-D reconstruction on diseased tissue samples for histopathological studying.

3.1 Brain Histology and Histopathology

Histology is the study of microscopic structure of tissue and cells under a microscope. A biological tissue sample is sliced to observe the inner structure and an embedding medium is usually needed for protection of the sample during cutting. The history of brain histology can be dated back to the 19th century when scientists discovered stains to apply to the nervous system [20]. Histopathology practiced in clinics adds in the pathological part where a biopsy(living tissue) or an autopsy(dead tissue) is taken from the patient to perform histology and make diagnosis from images under light microscopy [21]. A typical histopathology experiment is shown in **Fig. 3.1** [21-23]. We will introduce the basic principles of each step for the remaining section.

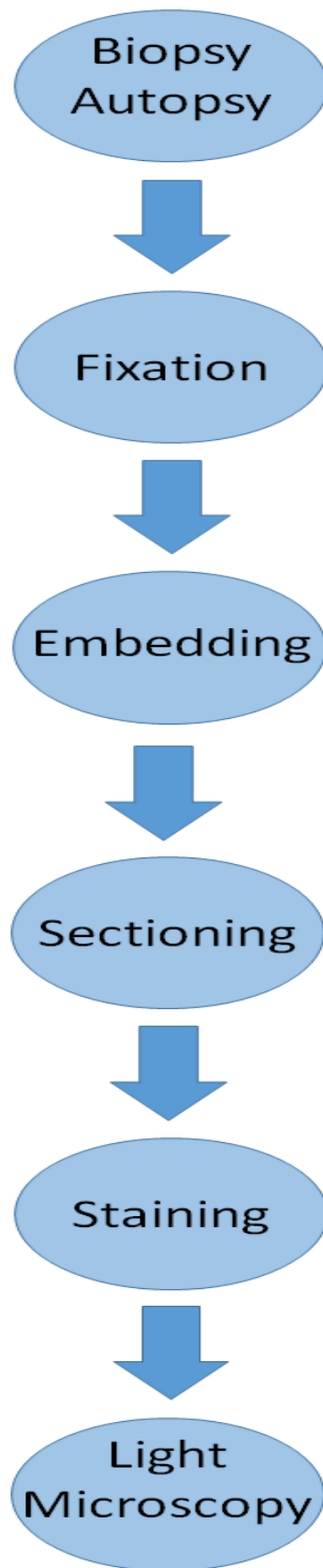



Fig. 3.1 Steps for Practicing Histopathology

3.1.1 Fixation



After obtaining a tissue sample from patient or postmortem tissue, the first thing that needs to be done is to immerse the tissue sample in a solution for fixation. The most commonly used fixative or fixing solution is formalin, which is a formaldehyde solution. The use of formalin to fix biological tissue samples were first introduced by Ferdinand Blum (1865 – 1959) in 1893 [24]. Now it is widely employed to preserve the morphology of fresh animal or human tissue. Formalin fixation induces crosslinking of amino acid side chains to maintain the original protein formation with more stability [25]. Furthermore, formaldehyde is considered a good fixative due to less distortion of biological tissue compared to other fixing solutions. **Fig. 3.2** briefly illustrates the mechanism of crosslinking by formaldehyde.

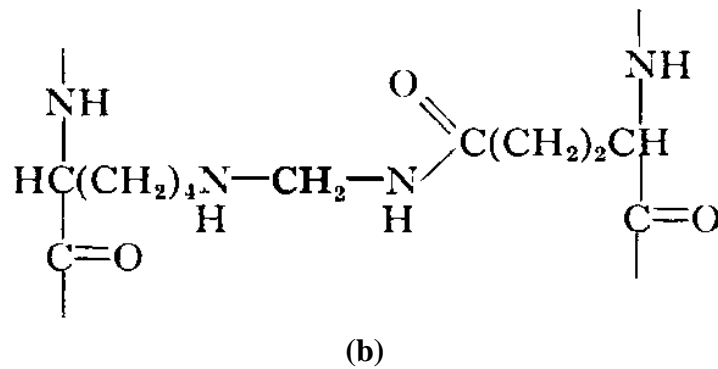
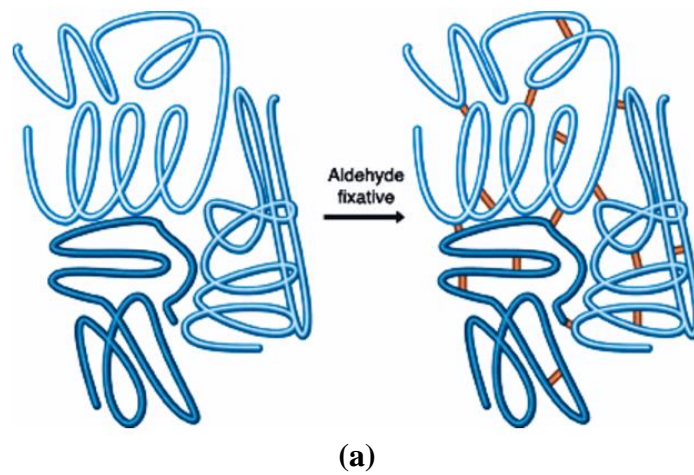
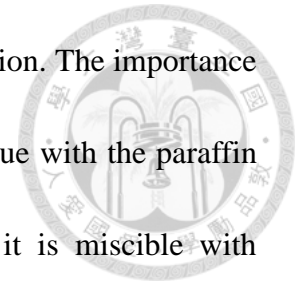


Fig. 3.2 Crosslinking mechanism of formaldehyde with protein. (a) Illustration of crosslinked protein. (b) The site of bonding. [25][26]

3.1.2 Paraffin Embedding

The embedding purpose for paraffin wax was applied first in the 19th century [21]. In order to embed a formalin fixed tissue into paraffin wax thoroughly without tissue separating from protecting paraffin during sectioning, dehydration and an empirically named “clearing” step should be performed first [23]. Dehydration is necessary for the penetration of the clearing agent to be used and can be done by ethanol, which is also known as alcohol. Serial incubation with raising ethanol concentration to prevent drastic

removal of water from the sample is needed for fear of tissue distortion. The importance of the clearing step is to improve the compatibility of the fixed tissue with the paraffin wax. Xylene is a commonly used agent for this purpose since it is miscible with paraffin.



3.1.3 Tissue Sectioning with Microtome

The idea of Microtome stems from using a blade or blade system to cut biological tissue into very thin slices. The first Microtome was invented in the 18th century by scientist Alexander Cummings (1733 – 1814) used to slice wood [27]. Now with the paraffin embedding technique and modified Microtome systems slices thinner than 10 μm can be made [6]. **Fig. 3.3** is a picture of a LEICA Microtome (RM2125 RTS) adopted by our laboratory for paraffin block sectioning.



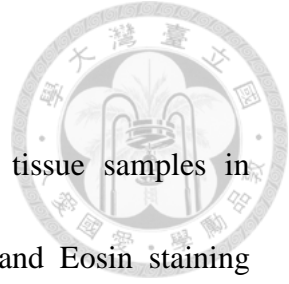
Fig. 3.3 LEICA Microtome RM2125 RTS

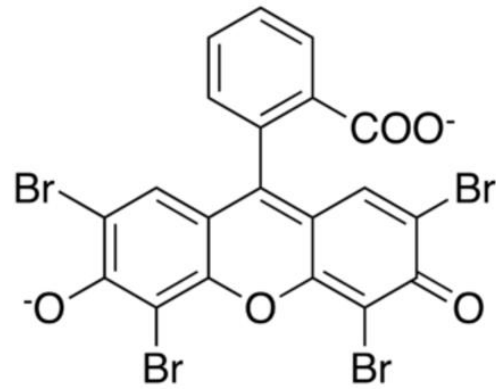
3.1.4 Hematoxylin and Eosin Staining

This is the most frequently used combination for staining tissue samples in histopathology. Termed H&E for abbreviation, the Hematoxylin and Eosin staining technique was first introduced in the 19th century and still serves as the golden standard for diagnosis in histopathology [21].

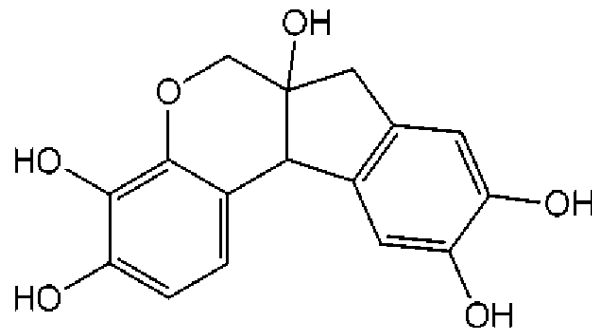
Fig. 3.4 shows the chemical structure of hematoxylin and eosin. Hematoxylin is a chemical extracted from the heartwood of the logwood tree. The oxidization of Hematoxylin produces Hematein which is the major substance that dyes the nucleus with dark blue color. DNA and RNA which are acidic with negative can be stained by the basic(positive charge) Hematoxylin solution.

Eosin on the other hand aims at the cytoplasm of cells and has different degree of staining on different structures causing distinguishable colors. Red, pink and orange are seen in eosin stained parts of a tissue micrograph. Protein in the cytoplasm are usually positively charged and so the acidic Eosin targets these places. Rehydration should be performed on paraffin embedded slices before the H&E stain and washing away of excess dye is done by tap water which is a factor for differentiation of the Eosin stain on different biological structures [23].





(a)



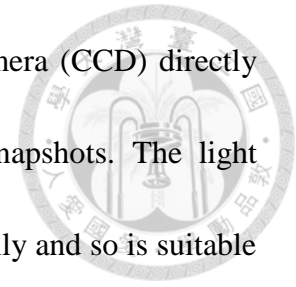
(b)

Fig. 3.4 Chemical formulae. (a) Eosin. (b) Hematoxylin

3.1.5 Light Microscopy

The light microscope or optical microscope functions to magnify small tissue samples through a series of lens with visible light to illuminate the field of view. The lens system requires essentially an eyepiece lens and an objective lens. When visible light travels through the tissue sample to the objective lens and eyepiece lens a magnified real image is acquired and can be seen by us through the eyepiece lens. The

real image can also be detected by a Charge-Coupled Device Camera (CCD) directly and transported to the computer for live recording or saving snapshots. The light microscope does not interact with the sample chemically or physically and so is suitable for observing biological samples that are usually fragile.



The Charge-Coupled Device (CCD) was invented by Willard S. Boyle (1924 – 2011) and George E. Smith (1930 –) at AT&T Bell Labs in Canada in 1969. The CCD acts as a sensitive photon detector and its surface is actually a grid filled with small dots. Each dot represents a light receptor and equals the smallest unit of an image called a pixel. The photons received by each pixel will be converted into one or a number of electrons as output which will be proportional to the light intensity displayed on the image. The total number of pixels defines the resolution of a digital CCD camera. That being said, pixel number is not the only thing that affects the image quality taken by the CCD camera. The CCD can be attached to a light microscope via a camera mount so that visible light can travel through the lenses to the CCD typical for a digital microscope.

3.2 Methods



3.2.1 Sample Preparation

Two human fetal brain samples, one with Holoprosencephaly(A10654) and one as control(A10642) were retrieved by National Taiwan University Hospital during surgery. The age of both samples were about 24 weeks of gestation. The Holoprosencephaly brain remained intact before fixation in 10% phosphate buffered formalin solution while the control brain had been dissected into tissue blocks during surgery. Both of the brain samples were fixed in 10% phosphate buffered formalin solution for over three months. A brief analysis of the Holoprosencephaly intact brain was done before experimenting with histology. We can see from **Fig. 3.5** that the corpus callosum is missing and that the brain also fails to separate into left and right hemispheres.

After considerable fixation samples went through dehydration and paraffin embedding before sectioning parallel to the coronal plane. Hematoxylin and Eosin were used to stain tissue samples for observing the structure through the light microscope. Work on paraffin embedding, sectioning and staining were done by National Taiwan University Hospital Staff.

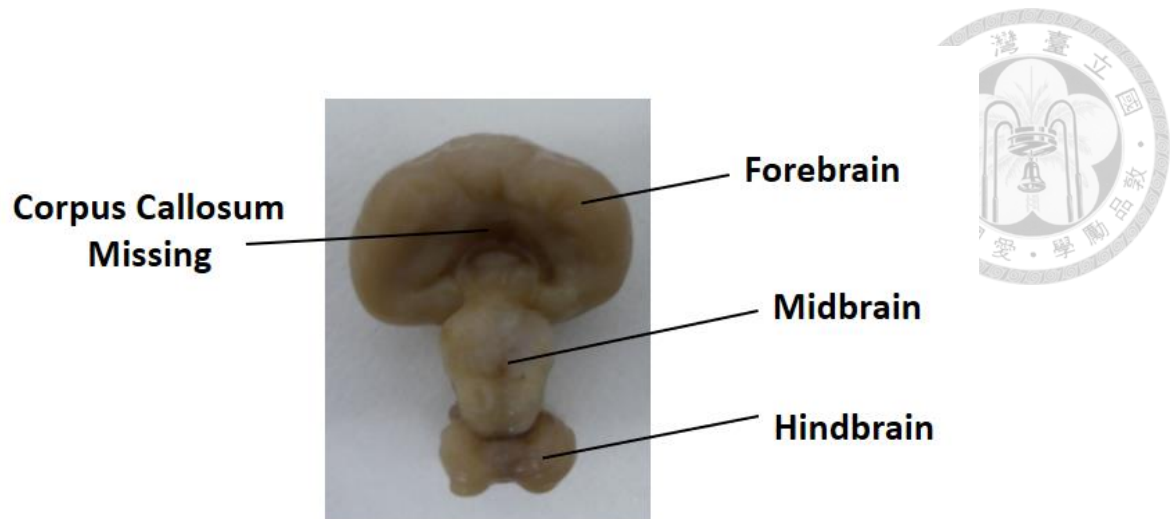


Fig. 3.5 Overview of the Holoprosencephaly(A10654) brain after fixation.

3.2.2 Experimental Setup for Light Microscopy

For imaging the H&E stained tissue samples on glass slides we combined the light microscope **Nikon TE-2000U** with the high resolution color CCD camera **Jenoptik CM5**. The objective lens **Nikon S Fluor 10X/0.5** was adopted to receive light and transfer onto the CCD camera for high resolution images. White light located on the light microscope system shone onto the sample and directly through the objective lens.

Fig. 3.6 illustrates the setup of the microscope-CCD system.

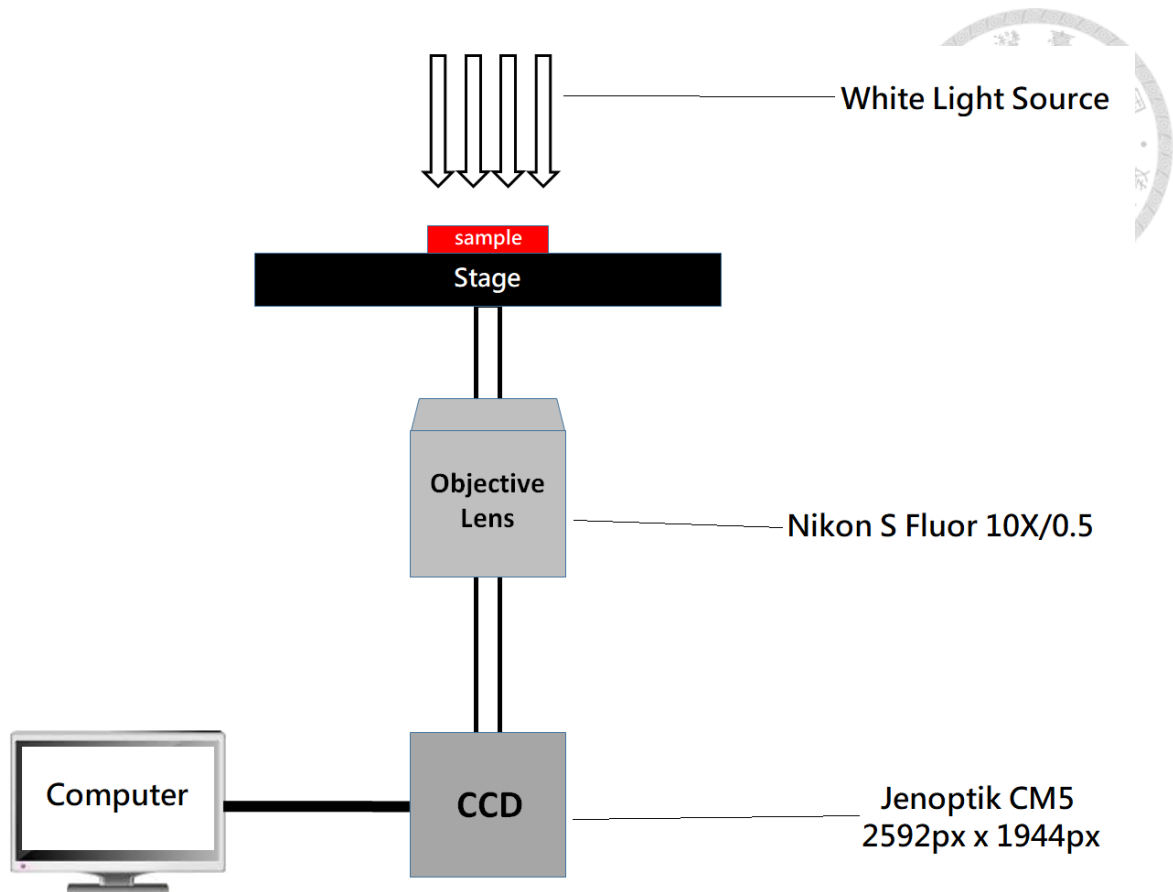


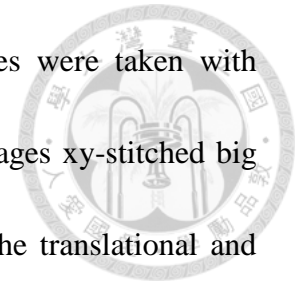
Fig. 3.6 Experimental setup for light microscope imaging.

3.2.3 Experiment Procedure

Sets of twenty consecutive paraffin-embedded slices of both A10654 and A10642 brain samples were prepared by Professor Pei-Hsin Huang’s laboratory staff, Department of Pathology, National Taiwan University Hospital.

For a set of twenty slices we first searched for locations on the neocortex that remained intact relative to places with serious distortion due to microtome cutting. We then scanned an area of about 3 – 5 mm² for stitching twenty consecutive slices together at the same location accurately. The view of the CCD camera connected to the **Nikon S**

Fluor 10X/0.5 was about 710 μm x 530 μm in size and images were taken with 2592 px x 1944 px high resolution. We basically took a 3x3 9 images xy-stitched big area scan to be sure of our location on every slice and adjusted the translational and rotational parameters by Image J software to align all twenty slices.



After stitching and aligning of images were done, we did 3-D image reconstruction on selected areas and calculated the cell density of a specific volume block. We used the Image J DropletFinder application as the tool for counting cell nuclei in a 3-D volume. The count divided by the volume analyzed then gives us the number density.

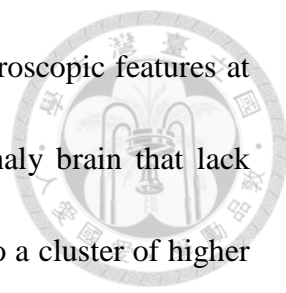
The hippocampus is observed and analyzed by the same method as for the neocortex which is mentioned in the previous paragraphs. The purpose of our methods would be to compare cell densities between the A10654 and A10642 fetal brain samples and look for abnormal 3-D structures within the Holoprosencephaly(A10654) brain.

3.3 Results and Discussion

We targeted the neocortex and the dentate gyrus in the hippocampus of the brain samples for studying 3-D structures. However, A10642 control brain was not intact after surgery and so we could not locate the hippocampal region since the dentate gyrus and CA regions were not spotted.

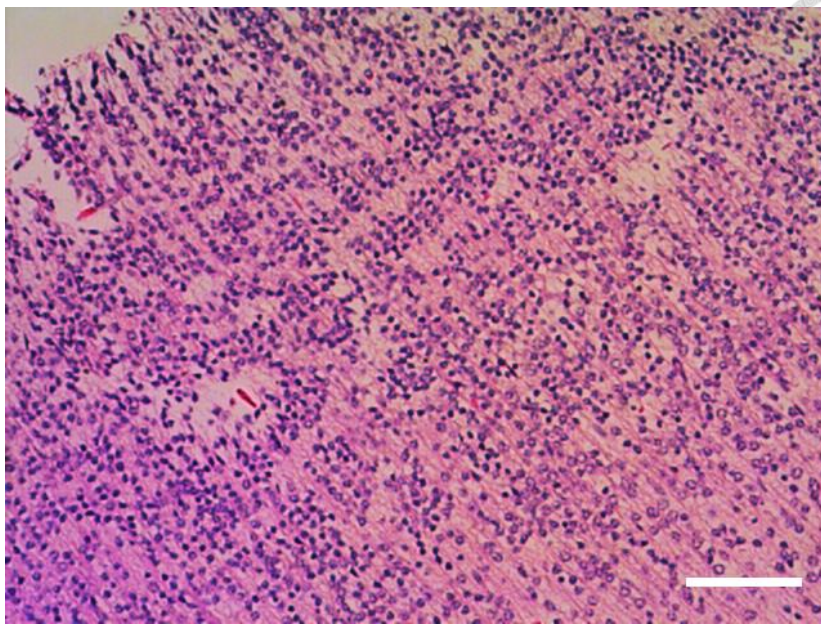
3.3.1 Histological Findings from 2-D Images

When taking a single image with the high resolution color CCD camera for

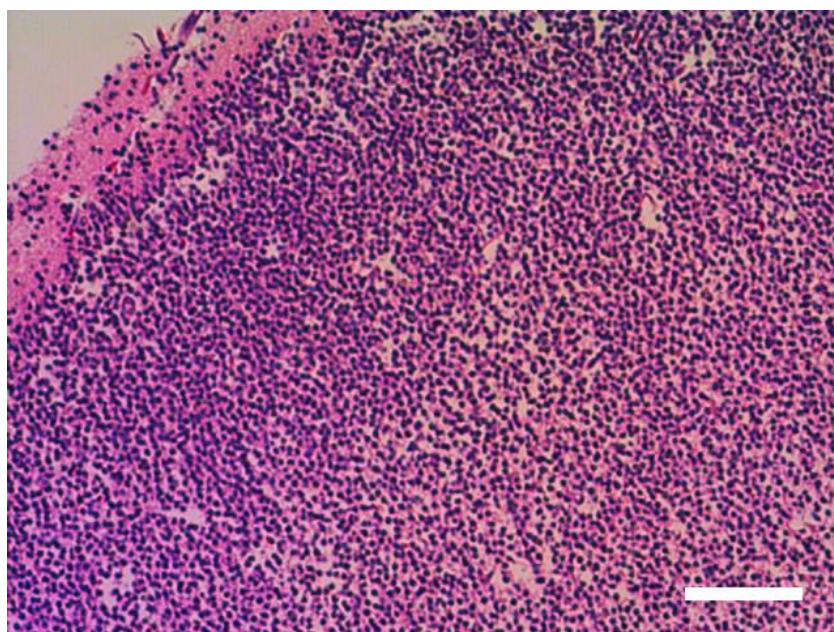


comparison of the two brain samples we noticed very different microscopic features at the cerebral neocortex. There were regions in the Holoprosencephaly brain that lack neuronal cells and also specific places where cells tend to crowd into a cluster of higher density. The regions with sparsity of cells are also known as paucicellular regions. With the control brain image we saw that the area considered was more uniform and the separation between the grey matter and white matter is very clear-cut. In contrast the layering of the Holoprosencephaly brain samples were unclear and separation between the white and grey matter was relatively poorer. **Fig. 3.7** shows the difference of micrographs of the two brain samples. The paucicellular regions are stained pink by eosin between the nuclei. Generally speaking the neocortex was thicker in control samples compared to the disordered samples.

As for the hippocampus in the Holoprosencephaly brain samples we saw abnormal cells in the granule cell layer of the dentate gyrus (see **Fig. 3.8**). The cell nuclei had a hollow center and looked like purple rings on the CCD color images. These nuclei were also present considerably in the neocortex of the same samples but not in the neocortex of the control brain samples.



(a)



(b)

Fig. 3.7 Comparison of neocortex structure between control and disordered brain stained with H&E. **(a)** A10654 neocortex. **(b)** A10642 neocortex. Scale Bar: 100 μ m

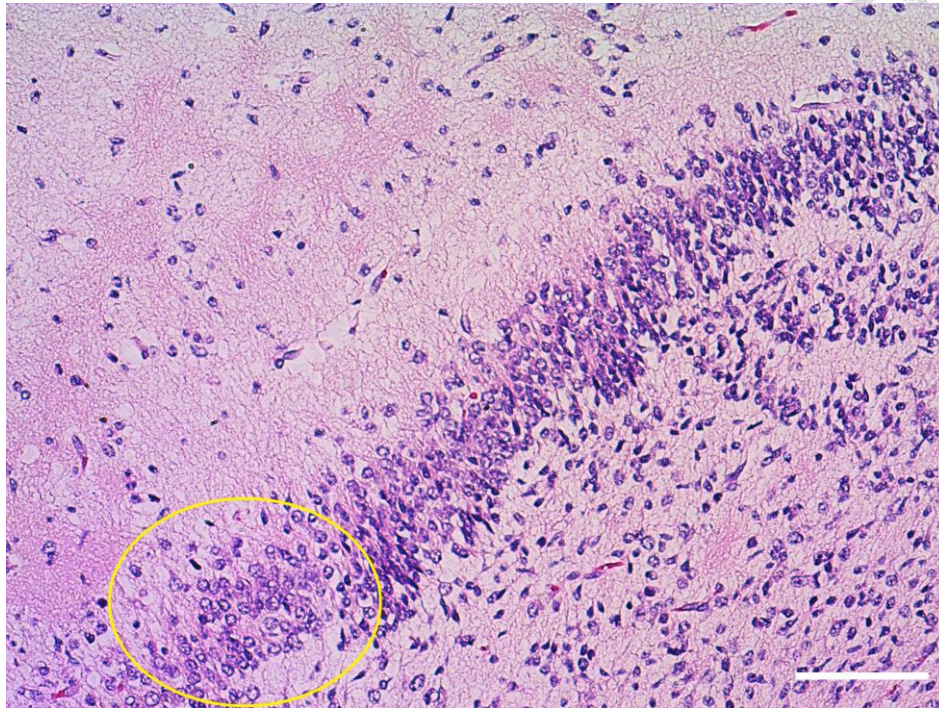


Fig. 3.8 Dentate gyrus, A10654. The high cell density region is the granule cell layer. The circled region contains a lot of abnormal nuclei hollow at the center.

Scale Bar: 100 μm

3.3.2 3-D Analysis of 20 Consecutive Tissue Slices

To do 3-D analysis we took twenty consecutive pictures at a specific location of a given sample set. We first compared the cell nuclei density in the neocortex of the control brain and disordered brain sample sets. We counted the cell nuclei within a volume block of 200 μm x 200 μm x 100 μm , where the last dimension is the thickness of the block in the z-direction due to stacking of 20 images each with 5 μm thickness. For the Holoprosencephaly brain we found that the number density of nuclei at the neocortex was 8.33×10^5 nuclei in each millimeter cube and that of the control brain 1.6515×10^6 .

The control brain has about twice the cell density of the Holoprosencephaly brain in the neocortex region. The figures below show the counting process and 3-D reconstruction.

We can see from the 3-D images that the Holoprosencephaly neocortex structure is less concrete and has several 3-D holes identifying regions without cell nuclei.

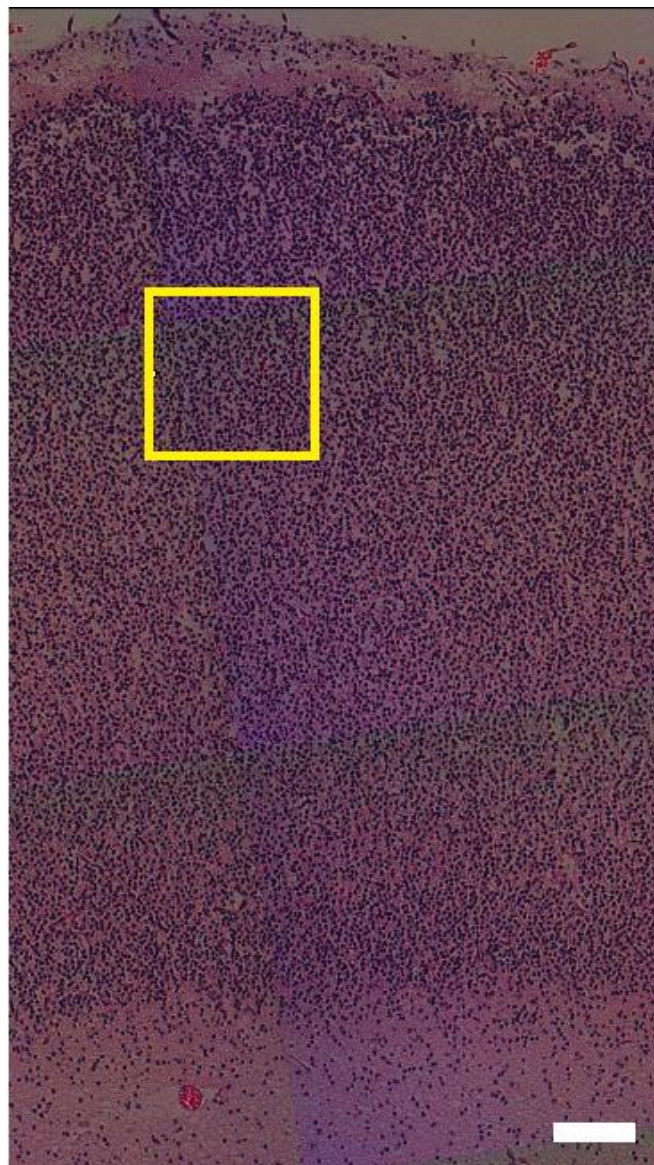


Fig. 3.9 (a)

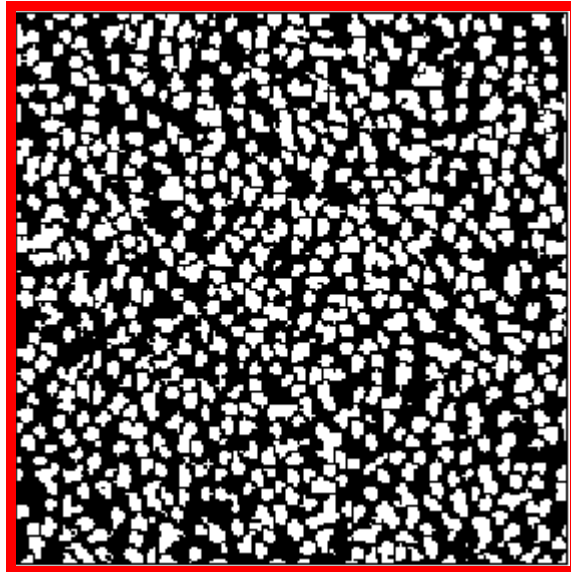


Fig. 3.9 (b)

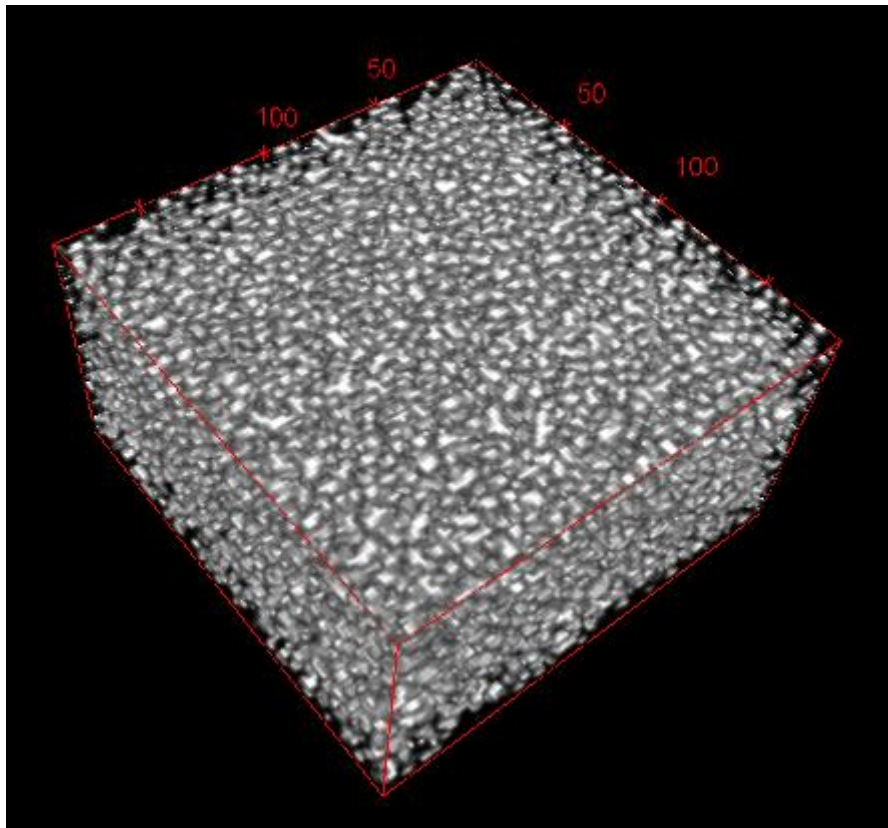


Fig. 3.9 (c)

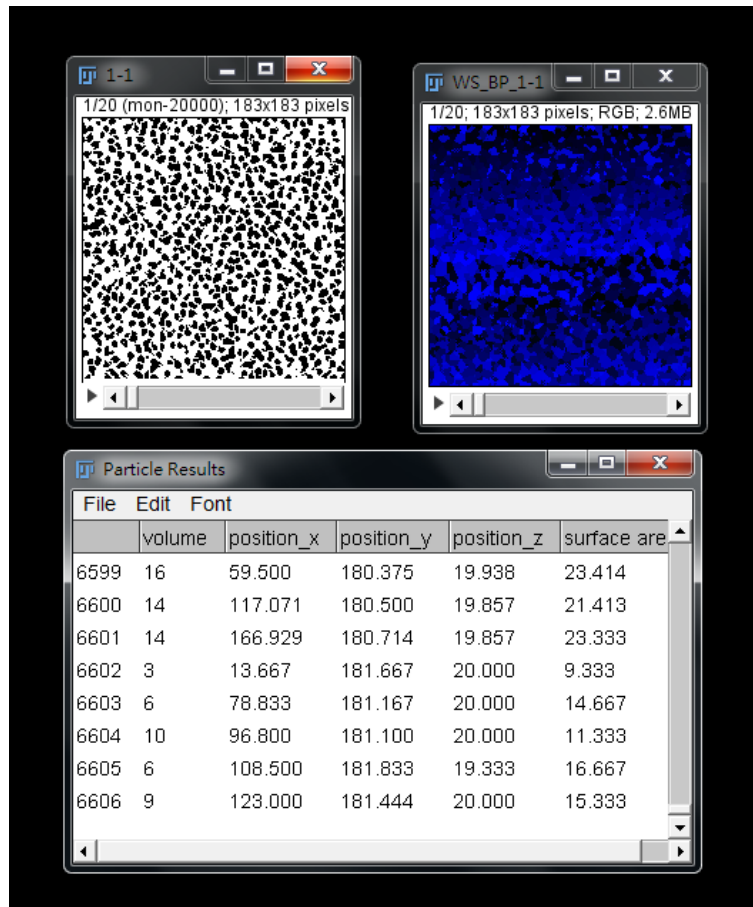


Fig. 3.9 (d)

Fig. 3.9 Results of control A10642. **(a)** Neocortex. The yellow boxed region with 200 μm x 200 μm size is chosen as a stack of twenty images for 3-D cell count. Scale bar: 100 μm . **(b)** Binary processed images of the boxed region. **(c)** 3-D reconstruction of **(b)**. **(d)** Cell counting application by Image J. The result is 6606 counts.

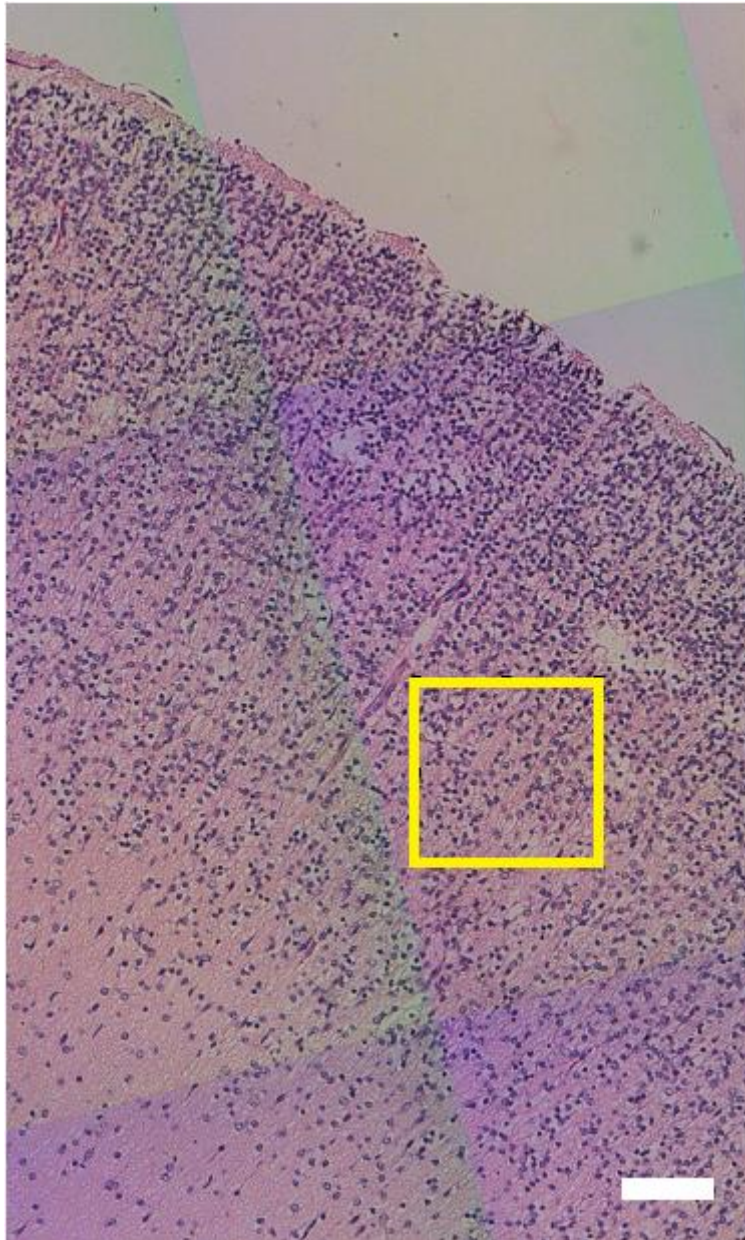


Fig. 3.10 (a)

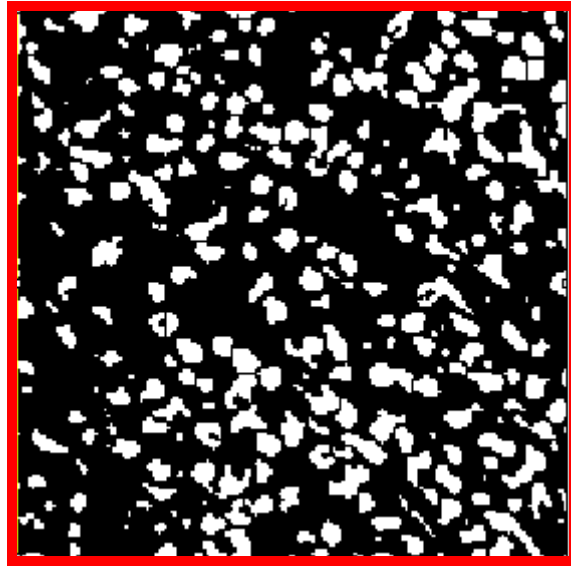


Fig. 3.10 (b)

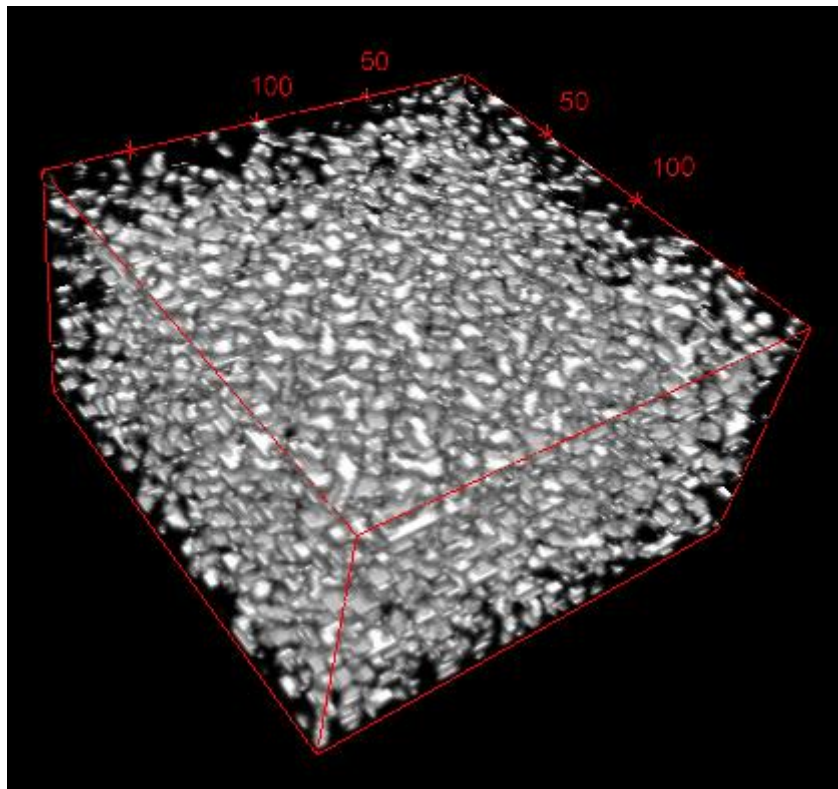


Fig. 3.10 (c)

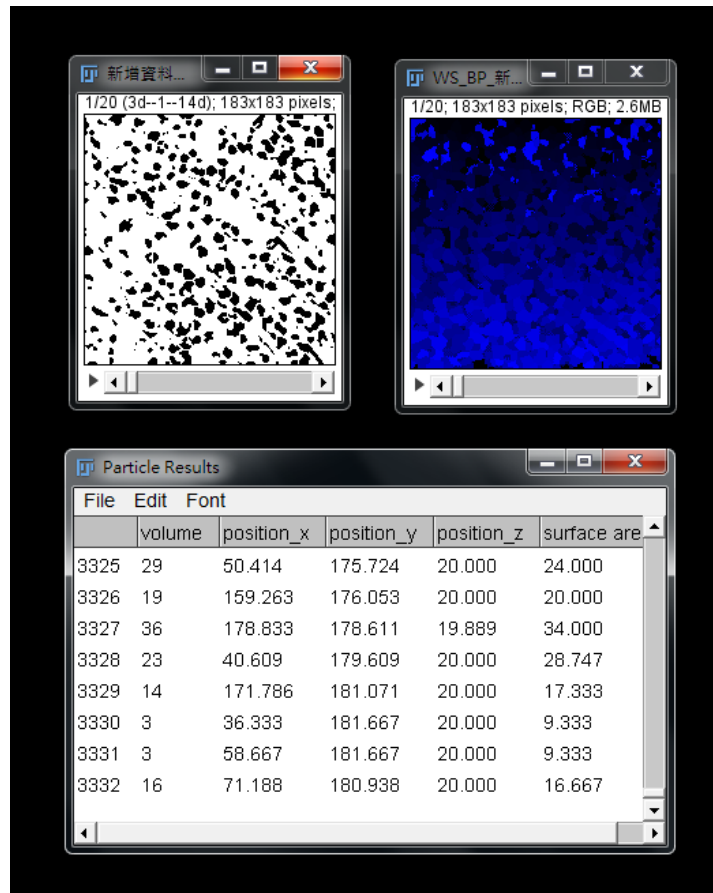


Fig. 3.10 (d)

Fig. 3.10 Results for the Holoprosencephaly A10654. **(a)** Neocortex. The yellow boxed region with 200 μm x 200 μm size is chosen as a stack of twenty images. Scale bar: 100 μm . **(b)** Binary processed images of the boxed region. **(c)** 3-D reconstruction of **(b)**. **(d)** Cell counting application by Image J. The result is 3332 counts.

For the hippocampus we also tried to calculate the cell nuclei density in the granule cell layer of the dentate gyrus. Although the cell count was 5014 yielding cell density 1.2535×10^6 per millimeter cube, the density should be higher since the granule cell layer is a band in 2-D image and the area chosen contains about half the volume that

does not belong to this layer. We also processed binary application to the twenty images and stacked the images together to see the morphological changes of the dentate gyrus due to different z-depth.

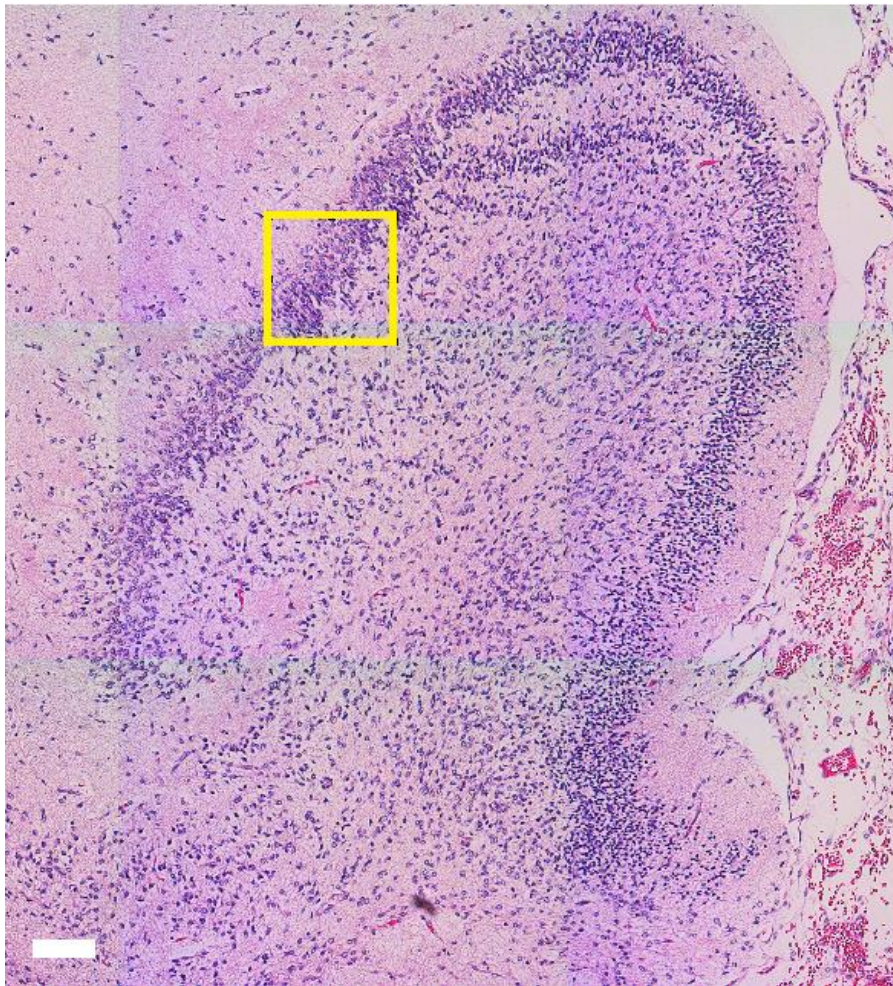
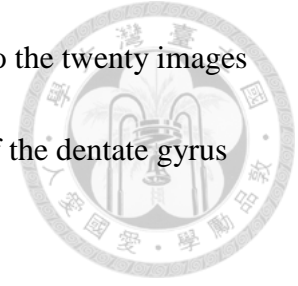


Fig. 3.11 (a)

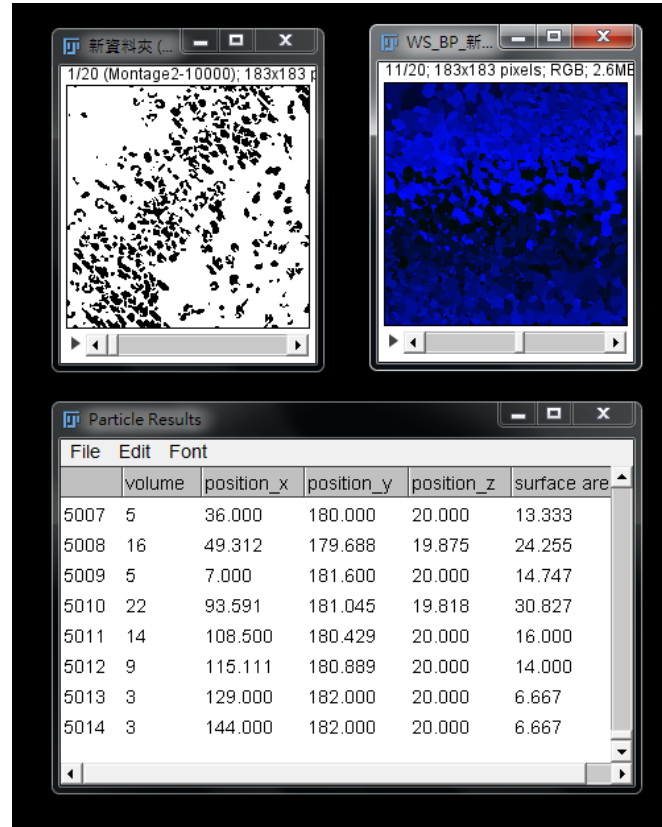


Fig. 3.11 (b)

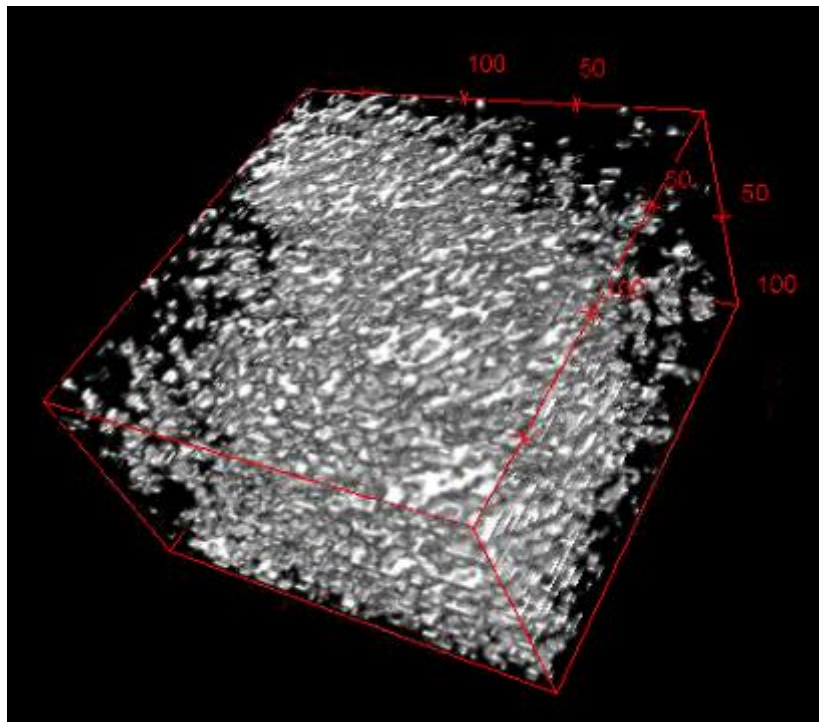


Fig. 3.11 (c)



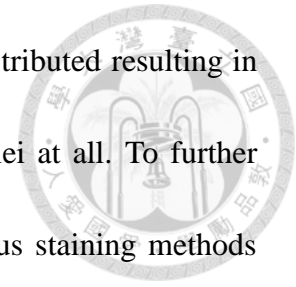
Fig. 3.11 (d)

Fig. 3.11 Results for the hippocampus of Holoprosencephaly A10654. **(a)** Dentate gyrus. The yellow boxed region with 200 μm x 200 μm size is chosen as a stack of twenty images. Scale bar: 100 μm . **(b)** Cell counting application by Image J. The result is 5014 counts. **(c)** 3-D reconstruction of boxed region. **(d)** 3-D stack of whole region. The left-bottom part of the dentate gyrus shows morphological changes due to z-depth.

3.3.3 Discussion

Calculation of the cell nuclei density in the neocortex of both brains showed that the density was significantly higher in the control sample than in the disordered sample.

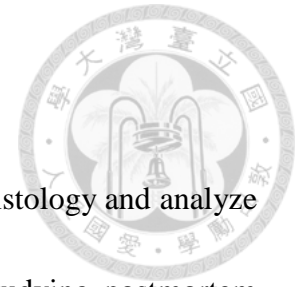
Also for the Holoprosencephaly brain, the nuclei were unevenly distributed resulting in some regions with higher nucleus density and others with no nuclei at all. To further study the cause of abnormal growth in the neocortex we need to use staining methods with more specific target such as antibody staining.



We aligned each image manually using the Image J software. This included rotating with less than 5 degrees to match adjacent images. Some common traits of samples such as blood vessels that went through the tissue block and was present on every slice were utilized as criteria for aligning. When aligning a twenty-image set we found that some images align really well while some don't. This may be due to the inconsistent tissue loss when cutting each slice [6]. Furthermore, there were also distortions such that the alignment of the same traits on two adjacent samples could not be optimized by image rotation and translation.

The 3-D reconstruction of images gave us more information such as identifying holes in the neocortex and seeing the morphological changes of the dentate gyrus. More information of the 3-D structure of the hippocampus could be shown if it is possible to raise the consecutive slice number to more than twenty slices. However, the quality of aligning could not be sufficiently addressed due to the fact that images have at best 5 μm resolution due to slicing and that H&E stains almost everything, making it difficult to distinguish between different cell nuclei.

Chapter 4 The Fresh tissue Approach

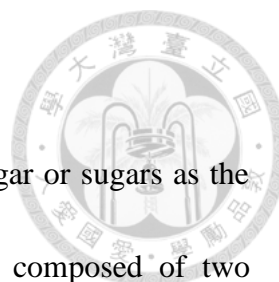


In this chapter we use an alternative way of performing brain histology and analyze the possibility of applying these methods to histopathology for studying postmortem brain with disorders such as the Holoprosencephaly case.

4.1 Overview of Alternative Histology

The main advantage of this approach to histology is that the only chemical reaction that alters the structure of the sample is the fixation process. Moreover, fixation helps preserve protein structure so we can say that the tissue sample is very close to its state at being alive before sectioning with a vibrating microtome. In some applications even the fixation process is skipped and fresh tissue samples are cut directly [28]. After fixation usually samples are embedded in warm molten agarose for protection during sectioning.

Another strength of this method is that samples need not be dehydrated and thus have a risk for serious distortion. This stems from the fact that the tissue sample is always processed in a hydrophilic environment. Agarose is compatible with water and the sectioning process with the oscillating blade is usually done in a water or buffer bath. Thus tissue samples and typically animal brain tissue samples carrying considerable amount of water can be well protected. On the other hand, embedding with paraffin requires changing the tissue to being hydrophobic and compatible with wax, which is done by dehydration and xylene clearing that cause distortion.



4.1.1 Agarose

Agarose is a polysaccharide meaning a polymer chain with sugar or sugars as the unit molecule(s). The unit of agarose polymer is a disaccharide composed of two different sugar monomers and the general origin from which agarose is extracted is seaweed. **Fig. 4.1** shows the general chemical structure of agarose. The solution of agarose powder in water or buffer has a melting point and a gelling point with different values, in contrast to the physical properties of a lot of substances which have the same melting/freezing point.

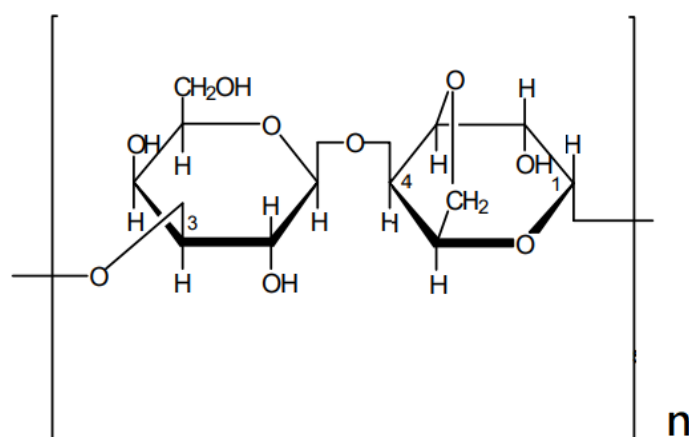


Fig. 4.1 Chemical structure of agarose.

Low melting point agarose is a modified version that reduces the melting point and mainly the gelling point. The fact that gelling point could be lower than 30°C gives us the advantage to embed animal tissue samples at temperature around 40°C since higher

temperature condition is not normal for live animals. The embedding role of low melting point agarose is seen in some publications with low concentration dissolved in phosphate buffered saline (PBS) [29-31]. We adapt a similar method to protect our brain samples with agarose to be prepared for the sectioning step.

4.1.2 The Pig Brain

To test the capability of the oscillating blade system on brain samples we used porcine brains as an alternative. The human brain and porcine brain have similar structure and gross anatomy [32], thus the choice of porcine brain for testing. For the same reason, the porcine brain is good model for studying human brain disorders. In **Fig. 4.2** we can see that the porcine brain has numerous gyri and sulci (lumps and fissures) structures that is similar to the adult human brain. Incidentally, there is easy access to the intact postmortem porcine brain at markets since it is a popular dish in Taiwan.



Fig. 4.2 Pig brain in 10% formalin. Notice the fissured surface that is similar to the human brain.

4.2 The Flexure-Based Oscillating Blade System

4.2.1 Design of the modified vibrating Microtome

The oscillating blade system is designed by Professor Shih Chih Chen from the Chinese University of Hong Kong. This sectioning system contains a flexure-based design to optimize the one dimensional movement of the vibrating blade [7]. **Fig. 4.3** illustrates the basic mechanism of the two flexures. Vibration activated by the motor is in general a three dimensional movement. The first flexure is very stiff in the in the y-direction and the second one very hard in the x-direction. Here the y-direction

represents the direction in which the sample moves towards the blade; the x-direction is the vibrating direction of the blade. This prevents coupling of motion in different directions and the vibrational movement of the blade is simplified. **Fig. 4.4** shows the actual form of the oscillating blade design from bird's eye view.

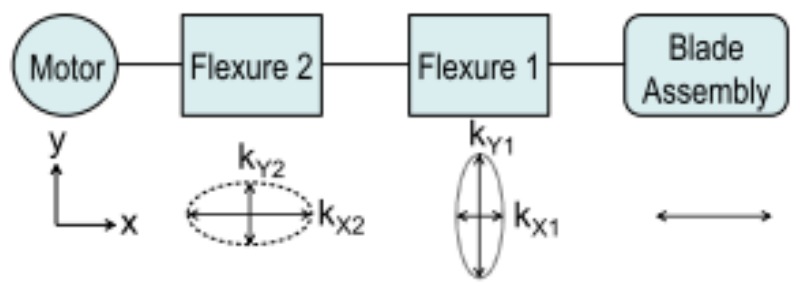
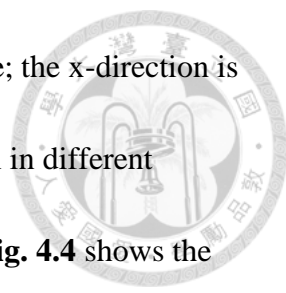


Fig. 4.3 Process of optimizing blade motion. The two serial flexures with different stiffness ratios cancel out unwanted motion in the y-direction. [7]

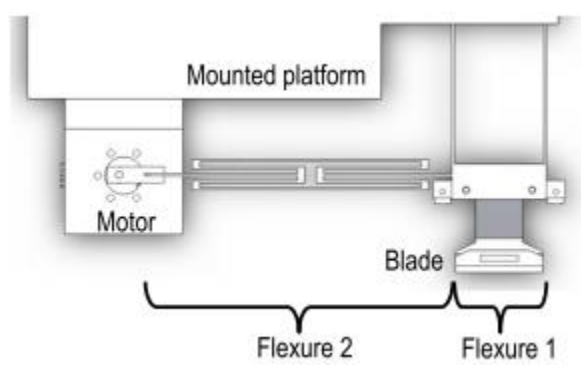


Fig. 4.4 Top view of the oscillating blade system. [7]



4.2.2 Cutting Parameters

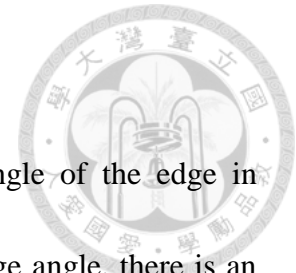
In theory based on classical mechanics, the higher the vibrating frequency the better the tissue sample is cut. Also, the slower the blade and tissue move against each other in the x direction the less distortion caused. For a given frequency, higher cutting amplitude should also improve cutting due to higher relative transverse speed between the blade and the sample.

The support for the sample is also a changeable parameter. Our primary support is agarose which might not be enough because agarose is soft. It is reported that the commercial Compresstome Vibratome and Leica Vibratome each have advantages and disadvantages compared to each other [28]. We want to test the effect of adding an aluminum ring outside the agarose for more structural support. The idea for additional support comes from the commercial Compresstome Vibratome with a specimen tube for holding the tissue sample.

4.2.3 Blade Material

The material for the oscillating blade is a very important factor of sectioning quality and is also a parameter since we can change the blade on the system. The three types of material we used for sectioning were steel, sapphire and tungsten carbide blades. These are the materials in use of Microtomy and have their advantages over

different tissue samples [33].



Generally, the stiffness or hardness of the blade and the angle of the edge in practice can alter the results of sectioning. When given a finite edge angle, there is an ideal angle for cutting [34]. **Fig 4.5** illustrates the consequence for blade angles too high or too low. Steel, tungsten carbide and sapphire have different hardness and thus different malleability since the two physical properties are inversely correlated. In general, high material stiffness results in low malleability, meaning more brittle and easier to break.

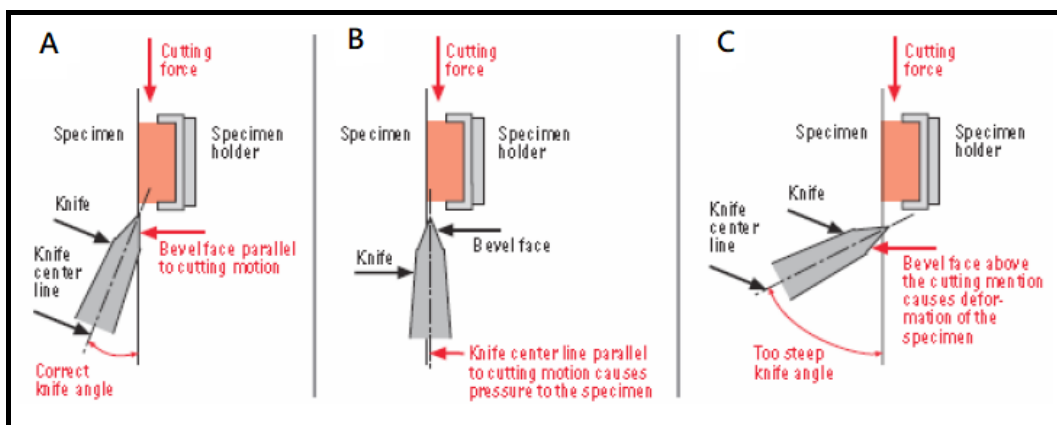


Fig. 4.5 A: Optimum knife angle. **B:** Angle too low; knife hits the sample surface. **C:** Angle too steep; sample slice above the knife is pushed. [34]

There are numerous ways to compare or even quantify the stiffness and hardness of different materials. The stiffness can be defined the Young's modulus as the ability of the material as a whole to withstand the pressure exerted. The Calculation of the Young's Modulus can be done with the following formula:

$$E \equiv \frac{F/A}{\Delta L/L}$$



E is Young's modulus; F is the force exerted on the material; A is the cross-sectional area; the denominator is the change of the length of the material perpendicular to the cross-sectional area divided by the original length. Young's modulus of Steel is about 200 GPa, of sapphire about 350 GPa, and of tungsten carbide about 700 GPa [35].

Another factor of blade material is the hardness which is defined as the ability of the material to withstand surface distortion such as abrasion or indentation. There is a method on comparing the hardness of different materials called Mohs scale. The relative hardness of two materials is addressed by scratching material A with the edge of material B and vice versa. The one that has a clearer mark meaning more vulnerable to the scratch is then defined as having lower hardness than the other material. The common scale used is shown in **Table 4.1**, with diamond having the highest index 10 as the hardest material. Tungsten carbide and sapphire have approximately the same index 9 and steel is indexed in a range 5 – 8 [36-37].

Hardnes Number	Original Scale
1	Talc
2	Gypsum
3	Calcite
4	Fluorite
5	Apatite
6	Orthoclase
7	Quartz
8	Topaz
9	Corundum
10	Diamond

Table 4.1 Mohs hardness scale. [36]

4.2.4 Surface Roughness

To study the surface tissue loss we can first investigate the surface characteristics of the tissue slice. The surface roughness is an important trait of the surface morphology that determines how two materials interact at the surfaces of contact [38].

There are numerous ways to address to the calculation of the surface roughness.

One way by using the following formula [39]:

$$R_q = \sqrt{\frac{1}{n} \sum_{i=1}^n y_i^2}$$

which is actually the standard deviation in statistics. R_q denotes the surface roughness; n is the number of points; y_i is the difference between each point and the mean. In this thesis we analyze the surface of the sliced tissue samples with calculating the tissue surface roughness for different blade material as the parameter.

4.3 Two-Photon Microscopy



The application of two-photon excitation to microscopic imaging had paved a new way to studying biology. Two-photon fluorescence microscopy is now a powerful tool that can scan images of biological tissue with considerable depth. This enables the study of biological function in live tissue [40] and also more efficiency in collecting 3-D image data since the imaging depth in the z-direction for a given sample is increased compared to other fluorescence microscopy techniques.

4.3.1 Fluorescence

Fluorescence is a stimulated emission phenomenon in that the fluorescent molecule is first excited by a photon and then emits another photon generally with a different frequency. The excited molecule undergoes non-radiative internal conversion or vibrational relaxation of states before jumping back to the ground state and emitting light. **Fig. 4.6** is a diagram illustrating the process of fluorescence, often called a Jablonski diagram.

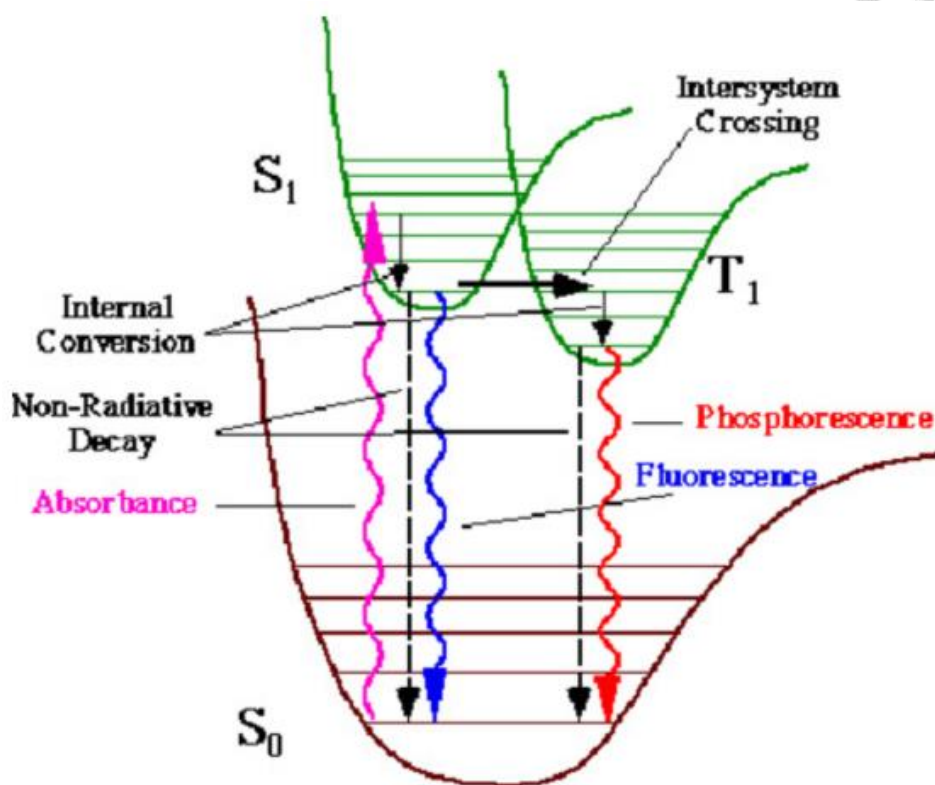


Fig. 4.6 Mechanism of fluorescence [41]

From the figure above we can see that the excited molecule can emit two kinds of radiation, named “Fluorescence” and “Phosphorescence”. Fluorescence occurs when the excited state due to absorbance of a photon is followed by internal conversion through the singlet states and eventually a jump to the ground state emitting light. Phosphorescence, on the other hand, describes the longer path the excited state returns to the ground state. An intersystem between the singlet and triplet states and internal conversion through the triplet states is experienced before going back to the ground state. In quantum mechanics however, this path is forbidden by total spin, thus a very low probability of jumping back to the ground state. The lifetime of fluorescence is

about $10^{-8} - 10^{-5}$ seconds and that of phosphorescence is $10^{-4} - 10^3$ due to the low probability of emitting light.



4.3.2 Two-Photon Fluorescence

Two-photon excitation compared to the one-photon case described in the previous section differs mainly in the excitation step. There is a virtual state between the ground and excited states and the first photon with half the energy is absorbed by the molecule which then temporarily stays in this state. The second photon with the same energy is absorbed subsequently and the molecule jumps to the excited state needed to undergo fluorescence. **Fig. 4.7** compares the Jablonski diagrams of the two mechanisms of fluorescence. The probability of a two-photon excitation process to occur is much lower than one-photon fluorescence, so a very strong intense light source such as a pulse laser is required to generate the two-photon excitation.

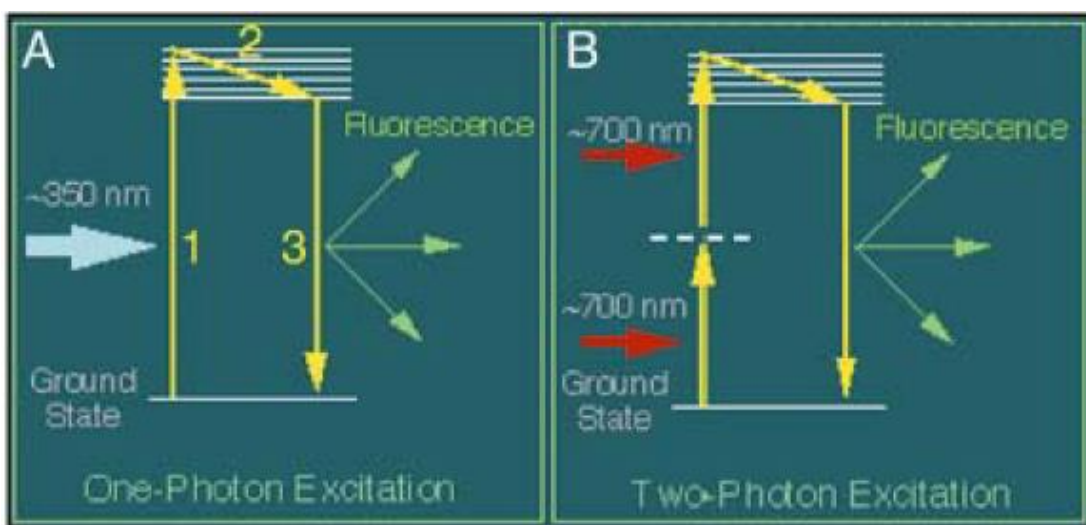


Fig. 4.7 Jablonski Diagrams. **A:** One-photon process ; **B:** Two-photon process [40]

The two-photon fluorescence microscopy technique is first described and forged in 1990 by Denk and his team [42]. The main strength of the technique is tight focusing compared to confocal fluorescence microscopy and better penetration depth of biological tissues since the laser light source is in the infrared spectrum (see **Fig. 4.8**). TPLSM is short for two-photon laser scanning microscopy and CLSM for confocal laser scanning microscopy. The point shaped focus compared to cone shape also implies less damage to the sample at places out of focus.

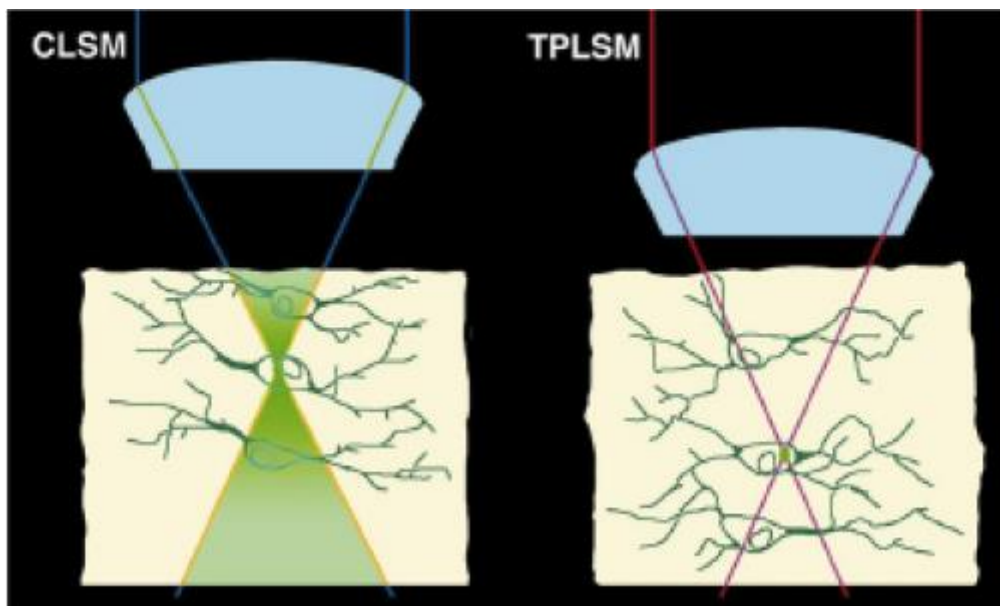
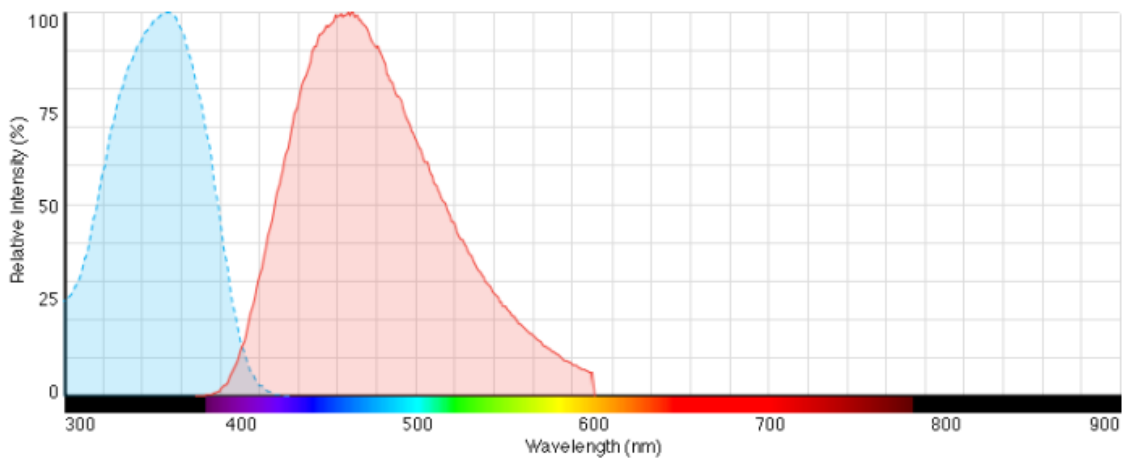


Fig. 4.8 TPLSM achieves better focus and penetration depth compared to CLSM. [40]

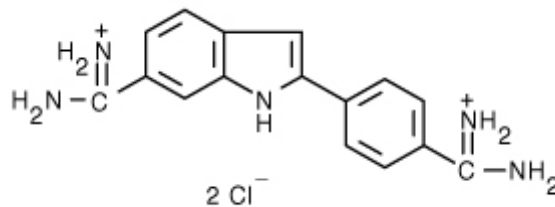
4.3.3 Fluorescent Dyes and DAPI

Fluorescent dyes are chemical dyes that have the ability to produce fluorescence when absorbing photons from an external light source. Each molecule is called a fluorophore unit and the more dense the molecules are crowded at the targeted

microstructure the brighter the fluorescence and hence the better the contrast to other non-targeted structures. DAPI (4',6-Diamidino-2-phenylindole) is a fluorescent dye that binds to the A-T regions of the DNA in cell nucleus efficiently. It can penetrate through the cell membrane to find target DNA and so the penetration depth of labeling tissue samples should not be a problem. The structure of the DAPI molecule enables it to absorb light near the ultraviolet region and emit blue light. The chemical structure and spectrum is shown in **Fig 4.9**.



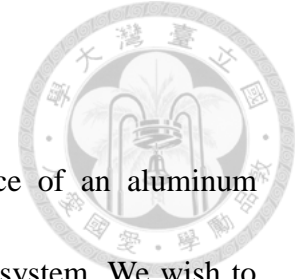
(a)



(b)

Fig. 4.9 DAPI. (a) Excitation emission spectrum. (b) Chemical formula. [43]

4.4 Methods



Our goal is to compare the blade material and the presence of an aluminum constraint on pig brain tissue being sliced by the oscillating blade system. We wish to find the best parameters for cutting brain by the system.

4.4.1 Sample preparation

Adult whole pig brains were purchased from the market. After the retrieval of the brain we had to take off the brain meninges at the surface using tweezers (see **Fig. 4.10**). Meninges serve as protection for the brain and is very hard to break apart. Leaving the meninges on the brain stops efficient contact with agarose and can cause cutting issues.

After the meninges were rid of we fixed the brain in 10% formalin for over a month. When fixing is sufficient took a sample from the brain and immerse in PBS for thirty minutes. We then took out the sample and dried it with Kimwipes before embedding it in molten agarose at about 40°C. After the agarose-sample block cooled down to about room temperature we stored it into a 4°C refrigerator for about thirty minutes prior to cutting.

For the test with adding an aluminum ring as constraint outside the agarose-sample block requires embedding the sample in the middle space of the ring (**Fig. 4.11**) to assure the close contact of the ring and the sample.



Fig. 4.10 Meninges on pig brain. The left half is after peeling off the meninges and the right half is before.

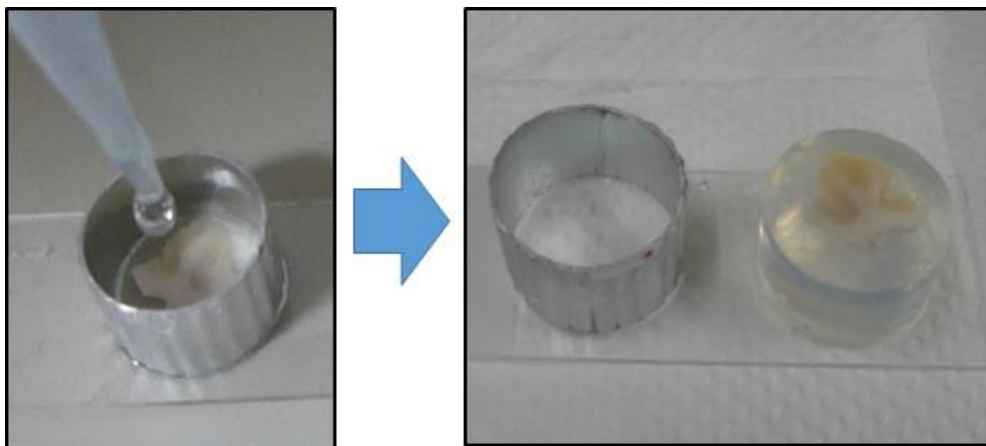


Fig. 4.11 Embedding with the constraint.

4.4.2 Setup of the Oscillating Blade System and Two-Photon LSM

The oscillating blade system based on the design of Prof. Shih-Chih Chen is shown in **Fig. 4.12**. The maximum vibration frequency the motor can generate is 80Hz and the

blade angle is adjustable. A water tank was attached to the moving xyz Prior stage and the sample was then fixed in the water tank by double-side tape and quick dry glue. Slices were achieved by moving the water tank towards the oscillating blade. The setup work of the system in our lab was done by Dr. Hung-Ming Lin.

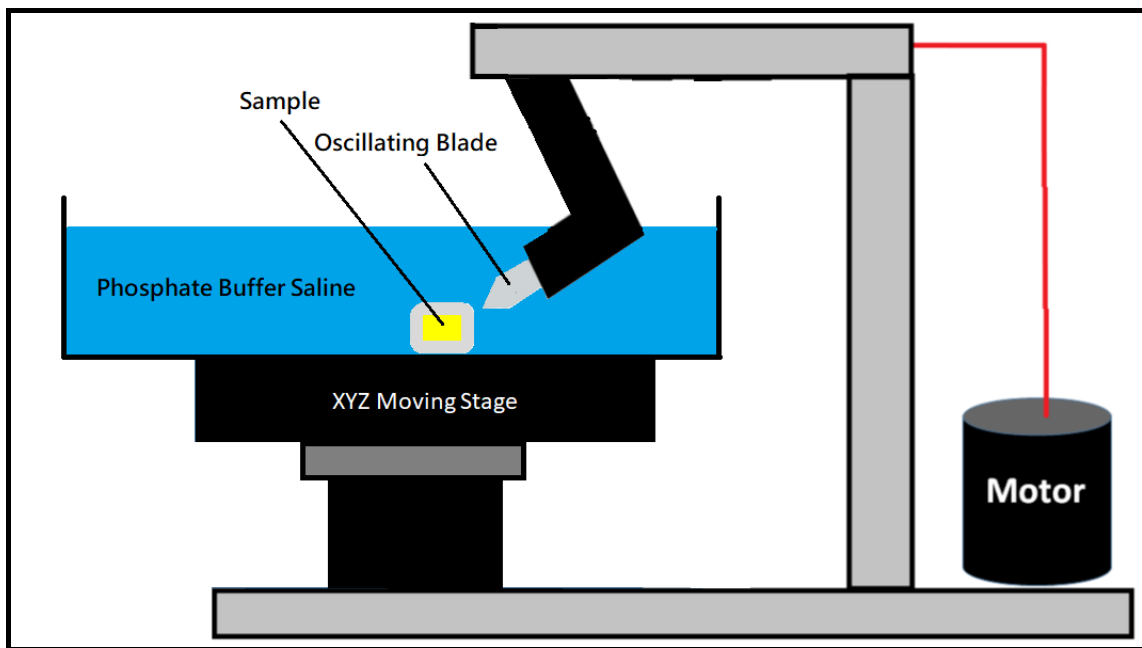


Fig. 4.12 The oscillating blade system.

The two-photon LSM system is depicted in **Fig. 4.13**. Two-photon excitation is generated by a pulsed laser (**Ti sapphire Tsunami, Spectra Physics, Mountain view, CA**) with the mode-lock technique to raise the intensity of the laser beam. The intensity of the beam can be adjusted by a linear polarizer. The beam goes through an x-y scanner and beam expander to scan the sample and obtain the highest numerical aperture possible from the objective lens. The incident beam goes through the **Nikon TE-2000U** microscope and the signal is reflected into the photo-multiplier tube, filtering the signal

with different channels. The objective lens used for the experiment is the **Nikon S Fluor 20X/0.75**.

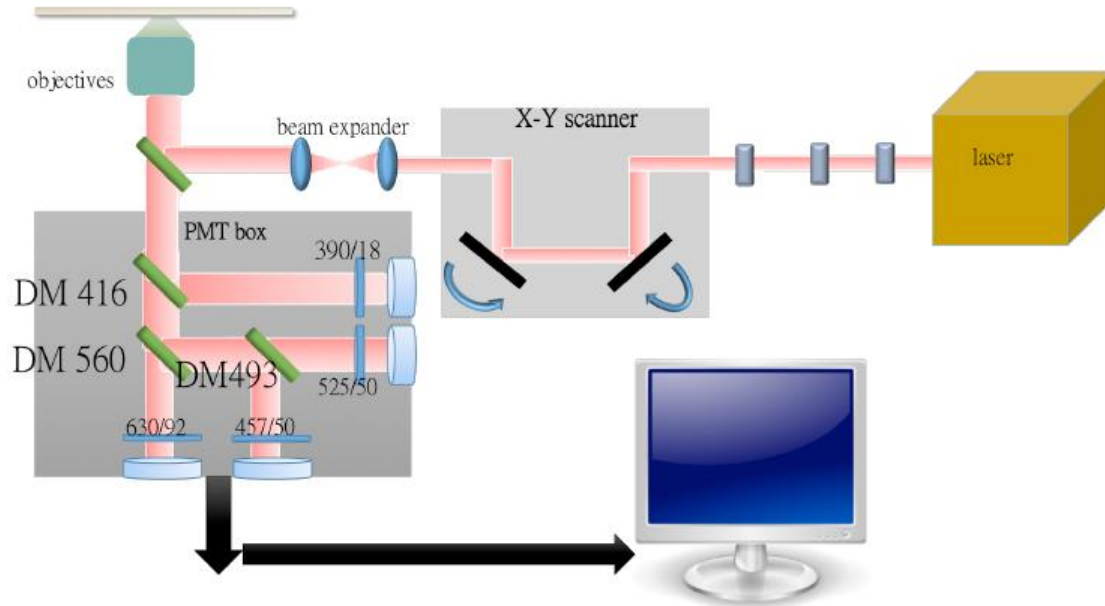


Fig. 4.13 Two-photon LSM system (figure provided by Ya-Lin Huang).

4.4.3 Experiment Procedure

We sliced the brain with steel, sapphire and tungsten carbide blades (**Fig. 4.14**). The blade angle was adjusted such that the bottom part of the blade does not touch the sample surface when cutting. The vibrating frequency of the blade is 80 Hz and after slicing we stained the samples' nuclei fluorescent with 150 μ M DAPI (4',6-Diamidino-2-phenylindole) and scanned an arbitrary location on the sample with changing z-depth by two-photon microscopy to obtain an image stack. Surface roughness calculation was done with the aid of Image J and Microsoft Excel.



(a)



(b)



(c)

Fig. 4.14 Experiment blades. (a) Steel blade. (b) Sapphire blade. (c) Tungsten carbide blade

4.5 Results and Discussion

We took serial images of a single position with $0.5 \mu\text{m}$ z-step and stacked 70 images together. We drew a line of segmentation with $120 \mu\text{m}$ length on the image to see the variation of the z-position of the surface on that line. The surface of the image was determined by Image J threshold application. The results were then inserted into Microsoft Excel for calculating the roughness. For each blade we show the surface

roughness R_q number and the image of the surface.



4.5.1 Steel Blade

Without constraint: $R_q = 3.4 \mu\text{m}$

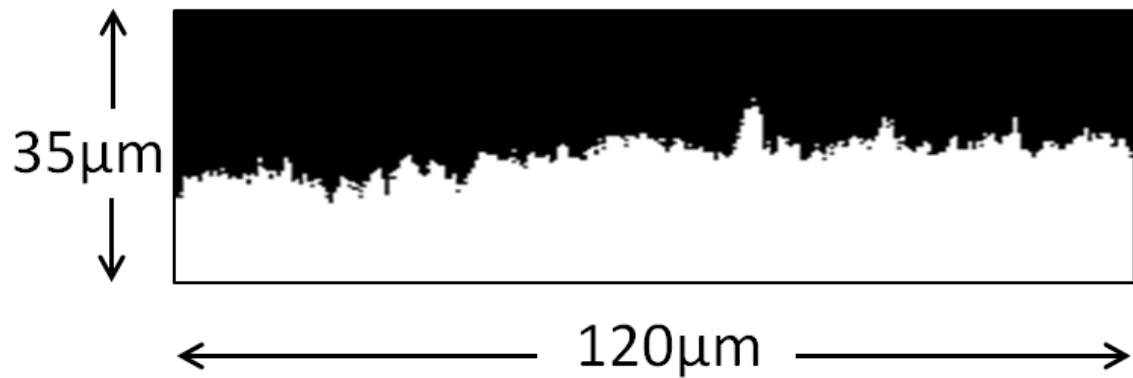


Fig. 4.15 Steel without constraint.

With constraint: $R_q = 1.7 \mu\text{m}$

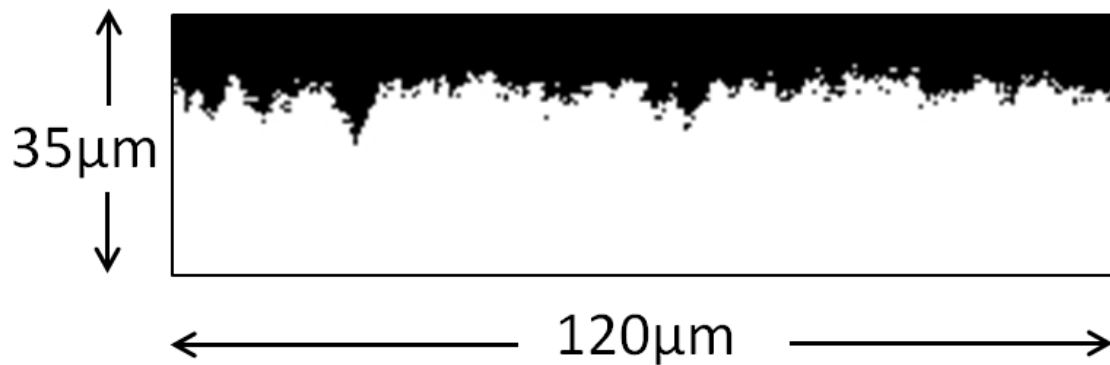


Fig. 4.16 Steel with constraint.

4.5.2 Sapphire Blade



Without constraint: $R_q = 1.6 \mu\text{m}$

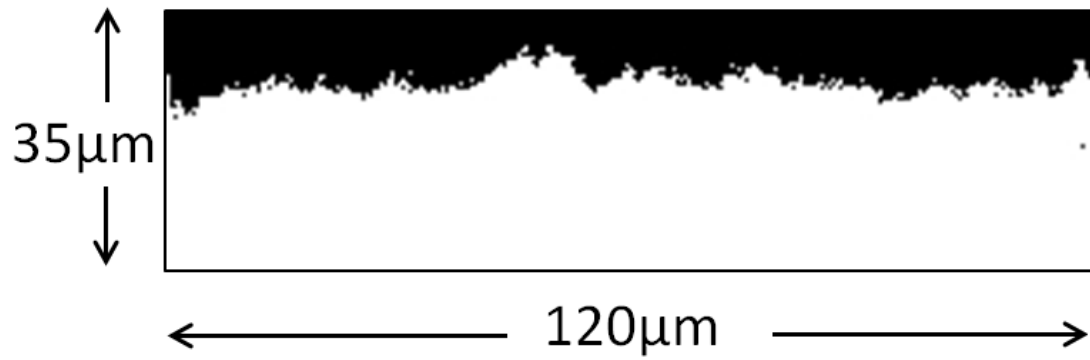


Fig. 4.17 Sapphire without constraint.

With constraint: $R_q = 1.5 \mu\text{m}$

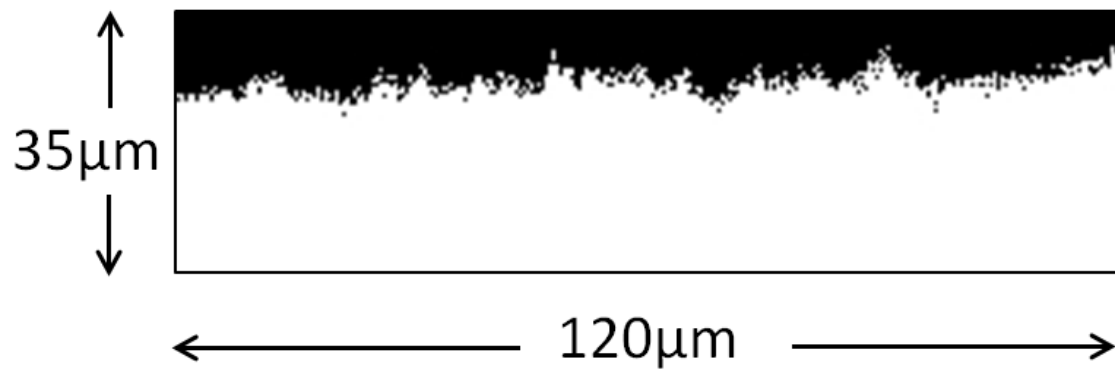


Fig. 4.18 Sapphire with constraint.

4.5.3 Tungsten Carbide Blade



Without constraint: $R_q = 1.1 \mu\text{m}$

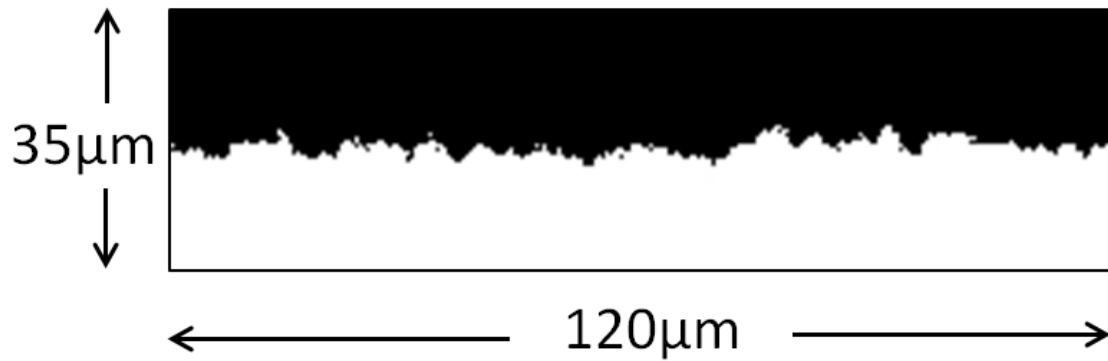


Fig. 4.19 Tungsten carbide without constraint.

With constraint: $R_q = 0.6 \mu\text{m}$

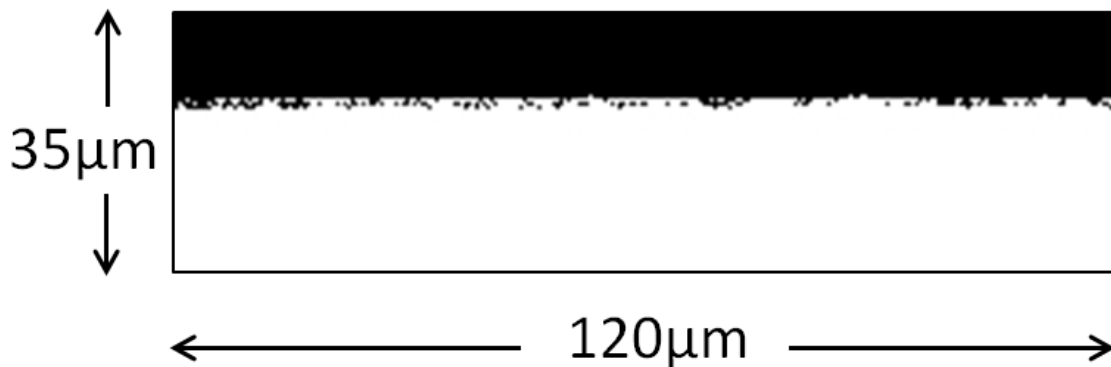
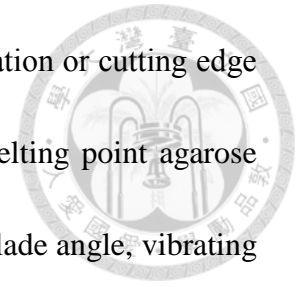


Fig. 4.20 Tungsten carbide with constraint.

4.5.4 Discussion

We found that the tungsten carbide blade cut best with surface roughness of about only one micrometer. Adding an aluminum ring as a constraint seemed to help with the cutting since the surface roughness was reduced on average. The steel blade cutting resulted in greater roughness than the other two materials. This might be due to lower

hardness and Young's modulus values inducing more blade deformation or cutting edge blunting. Pig brain samples seemed to work well with 4% low melting point agarose embedding and coronal plane cutting. We did not test the effect of blade angle, vibrating amplitude and vibrating frequency on the tissue surface roughness.



Chapter 5 Conclusion



5.1 Comparison of the Histology Techniques

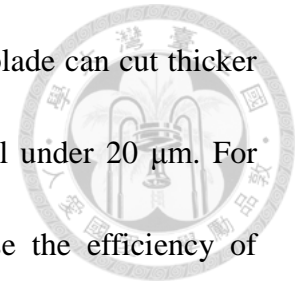
The study of Holoprosencephaly by the standard histology approach gives us insight into cell growth and distribution owing to high resolution images captured by the microscope-CCD system. 3-D reconstruction enhances the differences of the brain between the disease and control postmortem fetuses. The fresh tissue approach is successful in studying the mechanics of the pig brain and we now know that tungsten carbide is perhaps a better option for cutting brain samples.

On comparing the two approaches of studying the 3-D brain we found that the fresh tissue histology and standard histology have different advantages.

Embedding with agarose compared to embedding with paraffin does not change original tissue structure too drastically. Before embedding in paraffin samples need to be dehydrated and xylene-immersed in order to be miscible with paraffin wax. However, water is a major substance in most animal tissue and the dehydration process alters the tissue internal structure considerably. Agarose is hydrophilic so the dehydration process before embedding in it is not necessary. Agarose embedded samples however lose water by evaporation and so long period preservation is hard in contrast with paraffin slices.

The oscillating microtome technique and the non-vibrating microtome have

different strengths suitable for different situations. The oscillating blade can cut thicker samples above 100 μm while the microtome technique works well under 20 μm . For analyzing 3-D structures thicker slices should be needed to raise the efficiency of stitching of two different slices but thinner slices are easier to stain and preserve. Good preservation helps with controlling the experiment procedures and maintaining sample stability when a longer experiment period is needed.



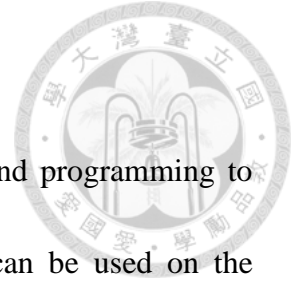
Imaging fluorescent stains with two-photon microscopy is the better option for 3-D analysis. White light obtains only 2-D information which is inapplicable to studying thick tissue samples. However, due to the high intensity of the laser beam, the power of the laser should be adjusted for imaging different tissue samples since tissue samples might be damaged if the laser is too strong.

5.2 Present Limitations and Future Work

For the standard approach, it is technically difficult and inefficient to make twenty consecutive slices and stitch twenty adjacent images just for analyzing 100 μm thickness. Also, the distortion and tissue loss will have a large impact on stitching difficulty and quality since every slice is in theory only 5 μm thick. Tissue loss is a major problem on both approaches that directly affects 3-D imaging. The fresh tissue approach is still limited to pig brain studies since we still don't have enough experience

for embedding and cutting the human brain.

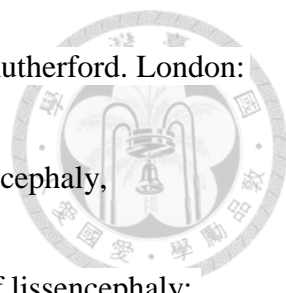
In the future it is important to work on automated designs and programming to improve the efficiency of cutting and imaging. Different stains can be used on the Holoprosencephaly brain samples to obtain more specific pathology and study the cause of the disease. To study the human brain with the fresh tissue approach we need to optimize the protocol for agarose embedding and fluorescent staining on targeted structures. We should test not only the surface structure but also the real tissue loss due to cutting for further improvement of the cutting parameters. The combination of oscillating blade cutting and two-photon microscopy should be able to give us answer about brain cutting tissue loss.

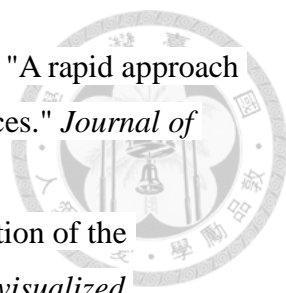


REFERENCE



- [1] Pandya, Sunil K. "Understanding brain, mind and soul: Contributions from neurology and neurosurgery." *Mens sana monographs* 9.1 (2011): 129.
- [2] World Health Organization. *Neurological Disorders: Public Health Challenges*. World Health Organization, 2006, Annex4.
- [3] Leoncini, Emanuele, et al. "Frequency of holoprosencephaly in the International Clearinghouse Birth Defects Surveillance Systems: searching for population variations." *Birth Defects Research Part A: Clinical and Molecular Teratology* 82.8 (2008): 585-591.
- [4] Lobo, I., and K. Zhaurova. "Birth defects: causes and statistics. Nature Education 1: 18." (2008).
- [5] Mizuguchi, M., and Y. Morimatsu. "Histopathological study of alobar holoprosencephaly." *Acta neuropathologica* 78.2 (1989): 176-182.
- [6] Masuda, Tomoyuki, et al. "How thick are the paraffin- embedded tissue sections routinely prepared in laboratory? A morphometric study using a confocal laser scanning microscope." *Pathology international* 48.3 (1998): 179-183.
- [7] Chen, Shih-Chi, et al. "DESIGN OF A PRECISION FLEXURE-BASED VIBRATION MICROTOME FOR WHOLE ORGAN IMAGING."
- [8] Bear, Mark F., Barry W. Connors, and Michael A. Paradiso, eds. *Neuroscience*. Vol. 2. Lippincott Williams & Wilkins, 2007.
- [9] Blumenfeld, Robert S., and Charan Ranganath. "Prefrontal cortex and long-term memory encoding: an integrative review of findings from neuropsychology and neuroimaging." *The Neuroscientist* 13.3 (2007): 280-291.
- [10] Garey, Laurence J. *Brodmann's 'localisation in the cerebral cortex'*. 1994.
- [11] Amaral, David G., Helen E. Scharfman, and Pierre Lavenex. "The dentate gyrus: fundamental neuroanatomical organization (dentate gyrus for dummies)." *Progress in brain research* 163 (2007): 3-790.
- [12] Gazzaniga, Michael S. "The split brain in man." *Scientific American* 217.2 (1967): 24-29.
- [13] E. Crisan, *Ventricles of the Brain*, Medscape 2016

- 
- [14] Bydder, Graeme M. *MRI of the Neonatal Brain*. Ed. Mary A. Rutherford. London: WB Saunders, 2002.
- [15] Stanley J. Swierzewski, "Cephalic disorders – Overview, Anencephaly, Colpocephaly." *Neurologychannel* 2008
- [16] Ghai, Sandeep, et al. "Prenatal US and MR imaging findings of lissencephaly: review of fetal cerebral sulcal development." *Radiographics* 26.2 (2006): 389-405.
- [17] G. Pilu, G. Malingier and R. Chaoui, *Holoprosencephaly*, VISUOG 2013
- [18] Cohen, M. Michael. "Holoprosencephaly: clinical, anatomic, and molecular dimensions." *Birth Defects Research Part A: Clinical and Molecular Teratology* 76.9 (2006): 658-673.
- [19] Ong, S., et al. "An epidemiological study of holoprosencephaly from a regional congenital anomaly register: 1995–2004." *Prenatal diagnosis* 27.4 (2007): 340-347.
- [20] A. Jeans and M. Esiri, "Brain histology." *Pract Neurol* 2008; 8: 303-310
- [21] Musumeci, Giuseppe. "Past, present and future: overview on histology and histopathology." (2014): 5.
- [22] G. Rolls, "An Introduction to Specimen Processing." Leica Biosystems
- [23] Bancroft, John D., and Marilyn Gamble, eds. *Theory and practice of histological techniques*. Elsevier Health Sciences, 2008.
- [24] Gatta, L. Benerini, et al. "Application of alternative fixatives to formalin in diagnostic pathology." *European journal of histochemistry: EJH* 56.2 (2012).
- [25] Baker J.R., *Principles of biological microtechnique: a study of fixation and dyeing*. Methuen & Co Ltd, London, 1958.
- [26] Copyright © 2011 National Diagnostics.
- [27] Quekett, John. *A practical treatise on the use of the microscope: including the different methods of preparing and examining animal, vegetable, and mineral structures*. Vol. 6. Bailliere, 1852.
- [28] Abdelaal, Hadia M., et al. "Comparison of Vibratome and Compressome sectioning of fresh primate lymphoid and genital tissues for in situ MHC-tetramer and immunofluorescence staining." *Biological procedures online* 17.1 (2015): 2.
- [29] John N. Abelson, Melvin I. Simon and P. Michael Conn, *Confocal Microscopy, Volume 307 (Methods in Enzymology) 1st Edition*, Chapter 32, p.576-589

- 
- [30] Selever, Jennifer, Jian-Qiang Kong, and Benjamin R. Arenkiel. "A rapid approach to high-resolution fluorescence imaging in semi-thick brain slices." *Journal of visualized experiments: JoVE* 53 (2011).
- [31] Shim, Katherine. "Vibratome sectioning for enhanced preservation of the cytoarchitecture of the mammalian organ of Corti." *Journal of visualized experiments: JoVE* 52 (2011).
- [32] V. Schmidt, *Comparative anatomy of the pig brain – an integrative magnetic resonance imaging (MRI) study of the porcine brain with special emphasis on the external morphology of the cerebral cortex*, Dissertation, University of Giessen (2014)
- [33] Mohammed, F., and T. F. Arishiya. "MICROTOMES AND MICROTOME KNIVES—A REVIEW AND PROPOSED CLASSIFICATION." *Annals of Dentistry* 19.2 (2013).
- [34] Charles W. Scouten, "Tips & Tricks in Sample Preparation: Knife angle in Microtomy." Leica Microsystems
- [35] Cardarelli, François. *Materials handbook: a concise desktop reference*. Springer Science & Business Media, 2008.
- [36] Copyright © Ted Pella, Inc., 1996-2017
- [37] Copyright © 2015 Valley Design Corp.
- [38] Zhai, C., et al. "The role of surface structure in normal contact stiffness." *Experimental Mechanics* 56.3 (2016): 359-368.
- [39] E. Paul Degarmo, J. Black and Ronald A. Kohser, *Materials and Processes in Manufacturing (9th ed.)*, Wiley (2003)
- [40] Mulligan, Sean J., et al. "Two-photon fluorescence microscopy: basic principles, advantages and risks." *Mod. Res. Educ. Top. Microsc* 2 (2007): 881-889.
- [41] Lee, Y.H. and Lakshminarayana, Polavarapu. "Recent advances in metal enhanced optical studies." *Cosmos*. 6. 167. (2010).
- [42] Denk, Winfried, James H. Strickler, and Watt W. Webb. "Two-photon laser scanning fluorescence microscopy." *Science* 248.4951 (1990): 73-76.
- [43] Copyright © 2017 Thermo Fisher Scientific inc.